Design of Voltage Controlled Oscillators at mmWave Frequencies for FMCW Radars

Thesis submitted in partial fulfillment
of the requirements for the degree of

(Master of Science in ***Electronics and Communication Engineering*** *by Research*

by

Srayan Sankar Chatterjee
2021702008
srayan.chatterjee@research.iiit.ac.in

International Institute of Information Technology
Hyderabad - 500 032, INDIA
December 2023

International Institute of Information Technology
Hyderabad, India

CERTIFICATE

It is certified that the work contained in this thesis, titled ***"Design of Voltage Controlled Oscillators at mmWave Frequencies for FMCW Radars"*** by Srayan Sankar Chatterjee, has been carried out under my supervision and is not submitted elsewhere for a degree.

Date

Advisor: Dr. Abhishek Srivastava.

To my friends and family!

Acknowledgements

I want to convey my deep and heartfelt gratitude to all those who have been an integral part of my journey in completing my master's thesis. First and foremost, I am immensely thankful to my dedicated thesis advisor, **Dr. Abhishek Srivastava**. His mentorship, patience, and unwavering support have played a pivotal role in shaping this work. Dr. Srivastava's insightful feedback and expert guidance have not only been instrumental but also truly inspiring throughout this academic endeavor.

To my family, I extend my sincere appreciation for their unwavering encouragement and steadfast belief in my abilities. Their love and unwavering support have served as the foundation of strength that has carried me through this challenging journey.

I would also like to express my gratitude to my dear friends and peers, specifically **Arpit Sahni**, **Adithya Sunil Edakkadan**, **Pranjal Mahajan**, and other members of our research group. Their presence created a supportive network that has offered valuable insights and a sense of camaraderie during this demanding yet ultimately rewarding period of my academic life.

Lastly, I am profoundly thankful to the academic and administrative staff at IIIT Hyderabad for their indispensable assistance and the resources they provided, which were crucial to the successful completion of this thesis.

This thesis project would not have been possible without the collective contributions of these exceptional individuals and institutions. I genuinely appreciate each and every one of you for being an integral part of this significant chapter in my academic journey. Your support and guidance have been invaluable, and I am deeply grateful for your unwavering belief in my capabilities.

Abstract

Recent advancements in the field of advanced driver assistance systems (ADAS) have led to increased demands for mmWave (millimeter-wave) radars operating within the 24 GHz and 77 GHz frequency bands. Among the various radar techniques, the Frequency Modulated Continuous Wave (FMCW) method has gained considerable popularity among mmWave radars. This approach relies on utilizing frequency synthesizers with low phase noise and high bandwidth to attain higher precision and accuracy in radar applications. Of particular interest in recent years is the growing demand for FMCW radars that operate within the 76-81 GHz frequency band due to their exceptional precision and accuracy, thanks to their wide bandwidth. These radars are well-suited for a range of applications, including autopilot systems and ADAS.

The primary focus of this thesis is to present research efforts aimed at enhancing the performance of FMCW radars at the circuit level, with a strong emphasis on the design, optimization, and simulation of Voltage-Controlled Oscillators (VCOs). VCOs play a critical role in radar systems, and two crucial design considerations are minimizing phase noise and reducing power consumption. These parameters directly impact the sensitivity and energy efficiency of the radar system. Various VCO topologies are explored, primarily based on LC oscillators, and comprehensive optimization endeavors are done to simultaneously minimize phase noise and power consumption. The VCO designs are implemented using TSMC 65 nm CMOS technology, allowing us to investigate innovative techniques for mitigating phase noise in VCOs.

In summary, this thesis encompasses recent developments in FMCW radar technology, specifically addressing improvements at the circuit level by focusing on the design and optimization of VCOs.

Contents

Chapter Page

1 Introduction . . . 1
  1.1 Problem Statement . . . 2
  1.2 Key Objectives . . . 2
  1.3 Key Contributions . . . 2
  1.4 Thesis Organisation . . . 3

2 Frequency Modulated Continuous Wave Radars . . . 4
  2.1 Types of Radar Systems . . . 4
    2.1.1 Pulsed Radars . . . 5
    2.1.2 Continous Wave (CW) Radars . . . 5
    2.1.3 Frequency modulated continous radar (FMCW) . . . 6
  2.2 Basic Principles of FMCW Radars . . . 6
  2.3 Advantages & Application areas of FMCW Radars . . . 7
    2.3.1 Advantages of FMCW Radars . . . 7
    2.3.2 Application Areas of FMCW radars . . . 8
      2.3.2.0.1 Automotive . . . 8
      2.3.2.0.2 Healthcare . . . 9

3 Design & Analysis of a Voltage Controlled Oscillator (VCO) for FMCW radars operating at mmWave frequency . . . 10
  3.1 Introduction . . . 10
  3.2 Low Phase Noise VCO Design Techniques . . . 11
  3.3 Proposed VCO Topology & Design Considerations . . . 13
    3.3.1 Pseudo sinusoidal waveform and high-Q load tank . . . 14
      3.3.1.0.1 Considerations for pseudo sinusoidal waveform generation 14
      3.3.1.0.2 Considerations for high-Q load tank . . . 14
    3.3.2 Transformer Design . . . 15
    3.3.3 Tuning range . . . 17
  3.4 Implementation & Simulation Results . . . 17

4 Design and Analysis of 20 GHz VCO based on Colpitts Topology . . . 21
  4.1 Introduction . . . 21
  4.2 The evolution of Colpitts oscillator . . . 21
  4.3 Proposed VCO Topology . . . 23
    4.3.1 Power Reduction . . . 23

4.3.2 Phase Noise Improvement 24
4.4 Implementation & Post Layout Simulation Results 25
4.4.1 Transformer Design Implementation 26
4.4.2 Post Layout Results 26

5 Design of Measurement Circuit & System Design using FMCW Radars 30
5.1 Design of Measurement Circuit 30
5.2 Object Classification using FMCW Radars 31

6 Research Contributions & Future Works 33
6.1 Research Contributions 33
6.2 Future Works 33

List of Figures

Figure Page

1.1 General Block Diagram of a Phase Locked Loop (PLL) 1

2.1 General Block Diagram of a Radar 4
2.2 Relation between TX and RX Waves in and FMCW Radar 7
2.3 FMCW Radar Application areas 8

3.1 (a) PLL block diagram for chirp generation (b) Noise Sources in LC-VCOs 10
3.2 (a) CS noise removal using a capacitive filter [12] (b) Use of transformer based VCO for generating sinusoidal and pseudo-sinusoidal waves [13] (c) Topology using implicit common mode impedance (d) DM and CM impedance peaks [14] 12
3.3 (a) Proposed VCO topology with $n < 1$ for mmWave operation (b)Transformer based resonator and its equivalent model 13
3.4 (a) f_h/f_l vs ζ for different k_m values (b) Q_{2f_0}/Q_{f_0} vs ζ for different Q_s/Q_p values . . 15
3.5 Gain vs ζ for first and second harmonics for (a) $n > 1$ (b) $n < 1$ 15
3.6 (a) Specifications of custom-designed transformer with $n < 1$ in HFSS (b) Layout in 65 nm CMOS technology (TSMC) of the proposed design 17
3.7 Post layout simulation results showing (a) phase and magnitude values of transformer's trans-impedance with Q_2 and Q_1 values (b) magnitude values of transformer's trans-impedance throughout the tuning range (c) transient waveform showing pseudo sinusoid behaviour at drain nodes and pure sinusoid at gate nodes (d) tuning range (e) phase noise (f) phase noise over the tuning range 18
3.8 Post layout phase noise variation at 1 MHz offset with variations in (a) supply voltage (b) process corners (c) temperature 19

4.1 (a) Colpitts oscillator (b) differential Colpitts oscillator [28](c) cross-coupled Colpitts oscillator [29] 22
4.2 (a) Introduction of PMOS cross-coupled structure for power reduction (b) pseudo-sinusoidal wave generation (c) proposed VCO topology 25
4.3 Proposed VCO with varactors and LC tuned buffer 25
4.4 (a) Custom-designed transformer in HFSS (b) layout of the proposed VCO in 65 nm CMOS technology (TSMC) 26
4.5 (a) Transient waveforms for V_{P1}, V_{N1}, and V_{OUT-} (b) transient waveforms for V_{P2}, V_{P2}, and V_{OUT+} (c) DFT plots for V_{P1}, V_{N1}, and V_{OUT-} (d) PPV plots for V_{P1} and V_{P2} (e) PPV plots for V_{N1} and V_{N2} 27

4.6 Post Layout simulations showing (a) tuning range (b) variation in phase noise across TR (c) variation in phase noise with temperature (d) variation in phase noise with supply (e) frequency variation with supply voltage (f) variation in phase noise across process corners (g) variation in phase noise with coupling coefficient (h) variation in phase noise with quality factor of L_2 28

5.1 (a) Designs for tapeout (b) CML Buffer (c) CML Latch (d) High frequency divider . . 30
5.2 (a) Test bench for post layout simulations (b) Differential VCO output at 20 GHz (c) Divided output at 40 MHz 31
5.3 Designed system for object classification using FMCW radars 31

List of Tables

Table Page

3.1 Quality factor Comparison for Multi & Single Turn Inductors at 20 GHz by using ASITIC 16
3.2 Performance Summary and Comparison with State of the Art 19

4.1 Performance Comparison of VCO1, VCO2, VCO3 Based on Schematic Simulations in 65nm CMOS 24
4.2 Post Layout Performance Summary and Comparison with Prior Works 29

Chapter 1

Introduction

Radar technology has experienced significant advancements over the years, and one noteworthy innovation is the Frequency Modulated Continuous Wave (FMCW) radar. This radar type stands out due to its high frequency, wide bandwidth, and short chirp time period, revolutionizing how we perceive and interact with our surroundings. It has become an indispensable tool in various sectors, ranging from automotive safety systems preventing accidents to environmental monitoring systems deepening our understanding of the Earth's atmosphere. At the core of FMCW radar systems lies the Phase locked loops (PLL). Figure 1.1 shows a general block diagram for a PLL. Voltage-Controlled Oscillator (VCO) (highlighted in figure 1.1) are a crucial component responsible for shaping radar signals that define the performance and capabilities of FMCW radar systems. As shown in the figure, the output of a VCO operating around 20 GHz is multiplied by a factor of 4 such that the final output is around 80 GHz. A distinguishing feature of VCOs is their ability to generate radio frequency signals with exceptional precision and stability. This precision in frequency manipulation plays a pivotal role in FMCW radar applications, where slight fluctuations in signal frequency are crucial for detecting and tracking objects with remarkable precision. This thesis is dedicated to offering a comprehensive grasp of VCO principles, technologies, and their implications, with a specific focus on enhancing phase noise reduction and minimizing power consumption.

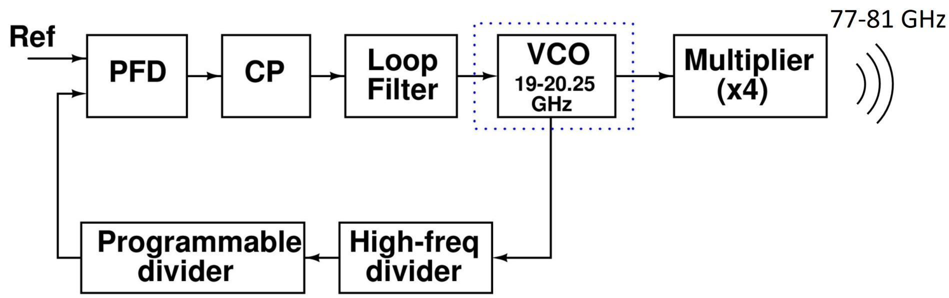

Figure 1.1: General Block Diagram of a Phase Locked Loop (PLL)

1.1 Problem Statement

The project's problem statement is defined as follows:

> *Problem Statement: To design Voltage-Controlled Oscillators (VCOs) with low phase noise and low power consumption and analyse their performance at 20 GHz*

In contemporary RF and Frequency-Modulated Continuous-Wave (FMCW) radar systems, the critical challenge is designing a low-power VCO that simultaneously minimizes phase noise. This problem statement aims to address the delicate balance between power efficiency and phase noise performance by proposing strategies to achieve both objectives concurrently. The project will entail a comprehensive literature review to gain a thorough understanding of the latest state-of-the-art VCO designs for reducing phase noise.

Subsequently, the research will involve extensive design and simulations for the implementation and enhancement of these VCO designs. Post-layout simulations will be employed to further refine and optimize these designs, ultimately achieving the dual goals of low power consumption and minimal phase noise in RF and radar systems. Additionally, the research will delve into a detailed mathematical discussion concerning FMCW radars. Furthermore, it will explore the system-level implementation of on-road object classification using FMCW radars as an integral aspect of the specified problem statement.

1.2 Key Objectives

- Develop new VCO topologies with low phase noise and power consumption operating in mmWave frequency region for FMCW radars.
- Develop benchmarking systems systems using commercially available FMCW radars that can be used in the domains of healthcare and security.

1.3 Key Contributions

The key contributions in this thesis are as follows:

- This thesis provides a comprehensive overview of different VCO topologies that have evolved over the last few decades for reducing phase noise.
- Two novel VCOs operating at 20 GHz have been designed and implemented using CMOS TSMC 65 nm. The thesis provides detailed discussion regarding the toplogy of these VCOs.
- The performance of these oscillators is assessed using post-layout results, emphasizing the robustness of these VCOs through these findings.

- An object classification system developed using commercially available FMCW radar is also discussed briefly in the thesis.

1.4 Thesis Organisation

Chapter 2 provides an overview of the architecture and fundamental operating principles of FMCW radars. It is followed by an extensive examination of the evolution of VCO topologies aimed at minimizing phase noise in Chapter 3. Additionally, thorough design and analysis of a VCO topology engineered for low phase noise operation at 20 GHz is also discussed in this chapter.

Chapter 4 focuses on the design and analysis of a VCO optimized for both low phase noise and low power consumption at the same frequency, 20 GHz. Both of these designs undergo validation through post-layout simulations utilizing CMOS TSMC 65nm technology. The results obtained underscore their robustness, demonstrating a high figure-of-merit.

Chapter 5 briefly outlines the design of measurement circuits done for tapeout along with some experimental work for classifying objects conducted using readily available radar components. Finally, Chapter 6 brings the thesis to a close and suggests potential avenues for future research. Furthermore, research contributions made by different members of our research group towards this thesis is also mentioned.

Chapter 2

Frequency Modulated Continuous Wave Radars

2.1 Types of Radar Systems

Figure 2.1 shows a general block diagram for radars. It consists of a transmitter and a receiver block which are built using fundamental circuits like oscillators, filters, amplifiers, ADCs etc. Radar technology encompasses a variety of specialized systems, each possessing distinct capabilities and serving specific purposes. These radar systems can generally be categorized into three primary groups: pulsed radar, continuous wave radar, and frequency modulated continuous wave radars.

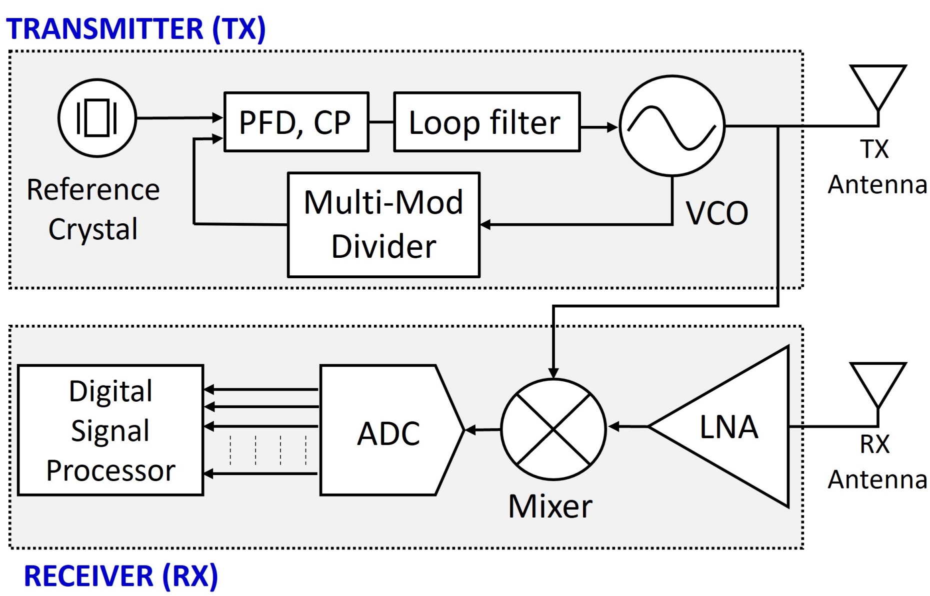

Figure 2.1: General Block Diagram of a Radar

2.1.1 Pulsed Radars

A pulsed radar system operates by emitting electromagnetic waves in discrete bursts or pulses, with intervals of time in between to monitor and detect any returning echoes of these transmitted pulses. This system serves as the basis for determining both the distance and direction of detected targets. The basic information about a detected target provided by a pulsed radar includes its range and direction. Range information is obtained by measuring the time it takes for the radar pulse to travel to the target and return as an echo. The directional information of the target is determined using the orientation of the radar's antenna at the moment it receives the echo.

Key parameters in pulsed radar operation include the pulse width (τ) or pulse duration (PD), which signifies the duration of each emitted radar pulse. The pulse repetition interval (PRI) refers to the time elapsed between the leading edge of one pulse and the leading edge of the next. This parameter essentially defines the time gap between consecutive radar pulses. The pulse repetition frequency (PRF) is the inverse of the PRI and indicates how frequently a radar system completes the process of transmitting a pulse and waiting for its echo. It is often expressed in hertz (Hz) and signifies the number of pulse-transmit-receive cycles that a radar can perform in one second. PRF is a critical parameter that influences a radar's performance, as it affects factors such as target detection, range resolution, and clutter rejection.

In summary, a pulsed radar system's fundamental characteristics include the emission of electromagnetic pulses separated by specific time intervals. These pulses are used to detect and characterize targets, with parameters like pulse width, pulse repetition interval, and pulse repetition frequency playing significant roles in the radar's functionality and performance.

2.1.2 Continous Wave (CW) Radars

In a continuous wave (CW) radar system, an electromagnetic wave is emitted with a constant, unbroken frequency. Unlike pulsed radar, where signals are sent out intermittently, in CW radar, the transmission is continuous. To gather information about potential targets, the radar receiver continually collects and analyzes the signals reflected back. For CW radar to function effectively, it necessitates the use of at least two separate antennas: one for transmission and another for reception. These antennas must be strategically positioned to maintain proper isolation between them. The purpose of this isolation is to prevent unwanted energy from the transmitted signal from leaking into the receiving antenna. If this leakage occurs, it can interfere with and contaminate the received signals, leading to inaccurate data and reduced radar performance.

However, achieving perfect isolation between the transmission and reception antennas is practically impossible. As a result, CW radar systems often employ lower transmit power compared to pulsed radars. This reduced power output helps mitigate the risk of signal leakage and interference between the antennas. While this approach enhances signal integrity, it also imposes limitations on the radar's operational range. CW radars are generally more suitable for short-range applications due to their reduced transmit power, making them less effective at detecting distant targets compared to pulsed radar systems.

In summary, continuous wave radar systems maintain a constant signal frequency and require two antennas for transmission and reception. Proper isolation between these antennas is essential to prevent signal interference. However, because achieving perfect isolation is challenging, CW radars often operate with lower transmit power, limiting their effective range and making them better suited for short-range radar applications.

2.1.3 Frequency modulated continous radar (FMCW)

Continuous wave (CW) radar encounters a significant limitation in its ability to determine the radial distance to a target. This limitation arises from the absence of time referencing within its signal. However, this challenge can be overcome with the application of frequency modulated continuous wave (FMCW) radar technology, which introduces a means to measure the radial range of stationary objects by periodically adjusting the frequency of the transmitted signal, thus creating a time reference within the signal. In FMCW radar, the fundamental principle involves altering the frequency of the transmitted signal gradually in a periodic fashion. This modulation process allows FMCW radar to effectively establish a time reference within the signal. Similar to pulsed radar systems, FMCW radar then utilizes the frequency difference between the transmitted and received signals to calculate the delay offset. This delay offset corresponds to the time taken for the signal to travel to the target and back, enabling the radar to determine the target's radial range accurately. FMCW radar systems have the flexibility to transmit signals with various frequency modulation patterns, but in practice, simpler approaches such as ramp and triangular modulation are commonly employed. These modulation patterns simplify the processing of received signals and facilitate precise distance, velocity, and angle measurements.

2.2 Basic Principles of FMCW Radars

This section delves into the fundamental operational principles of FMCW radar systems used to detect both range and velocity. As discussed earlier, the electromagnetic waves generated by these radars are modulated in frequency domain i.e. their frequency increases (or even decreases) gradually with time. This is illustrated in Figure 2.2. Generally, FMCW radars with high chirp (frequency modulated wave) bandwidth and steep slope provide increased precision.

When an object is situated at a distance x from the radar transceiver, the time disparity between the transmitted and reflected waves can be expressed as $\Delta t = 2x/c$, where c represents the speed of light. The beat frequency, denoted as Δf, between the transmitted and reflected waves, is directly related to Δt and is expressed as $\Delta f = k_f \Delta t$, where k_f signifies the chirp slope, as depicted in Figure 2.2.

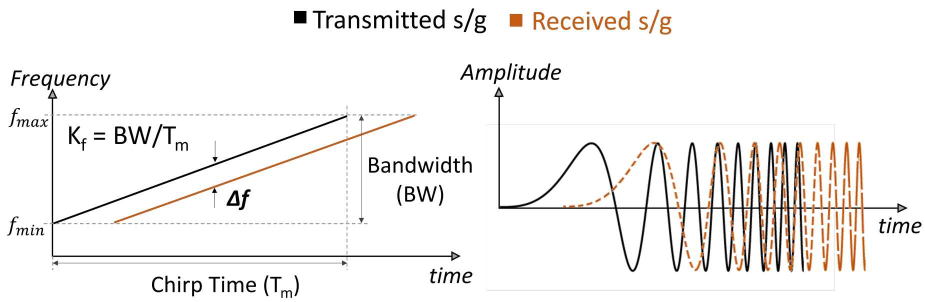

Figure 2.2: Relation between TX and RX Waves in and FMCW Radar

The range and velocity of the target are related to the beat frequency as

$$\Delta f = k_f 2x/c + 2f_c v/c \tag{2.1}$$

where f_c is the centre frequency of the chirp sweep and v is the relative velocity between the target and the transceiver.
Enhancing the chirp bandwidth enhances both the system's range and velocity resolution. Similarly, reducing the chirp time period T_m accomplishes the same goal. Furthermore, decreasing T_m allows for the effective resolution of multiple targets since the beat tones associated with each target will exhibit greater frequency separation [1].

2.3 Advantages & Application areas of FMCW Radars

This section begins by exploring the key benefits of FMCW radars, followed by a brief examination of their various application domains.

2.3.1 Advantages of FMCW Radars

The following are some of the major advantages of FMCW Radars:

1. FMCW radar sensors distinguish themselves from vision and LiDAR-based sensors [2] by maintaining their performance regardless of environmental conditions like rain, smog, dust, fog, or snow.

2. By utilizing compact antennas (whose form factor decreases due to the high operational frequency) and narrow beams, it becomes possible to track objects at low elevation angles effectively. This approach also helps in minimizing interference from clutter, delivering high-resolution data for nearby airborne targets, and achieving precise angle resolution for regional imaging and target monitoring purposes.

3. Achieving a high information rate is feasible thanks to high bandwidths. The use of either narrow pulses or signals with broad-frequency modulation enables the extraction of intricate structural details from the target, while also enhancing the system's resilience to interference, thus enabling it to effectively combat mutual interference. Furthermore, it provides excellent long-distance resolution, streamlining the task of precise target tracking and identification.

4. These radar systems demonstrate outstanding performance in the detection and identification of slowly moving objects as well as vibrating targets. They effectively utilize the Doppler frequency characteristics of these targets to facilitate accurate target recognition.

5. Modern stealth aircraft utilize specialized absorbent materials to mitigate centimeter wave detection. However, research has shown that millimeter wave radar can induce multiple strong electromagnetic reflections on stealthy targets, substantially reducing their stealth effectiveness. This underscores the potential of FMCW (millimeter wave) radars to counteract stealth countermeasures.

2.3.2 Application Areas of FMCW radars

Illustrated in Figure 2.3, FMCW radars find prominent applications in two key sectors: healthcare and the automotive industry. A brief overview of these applications is provided in the following paragraphs.

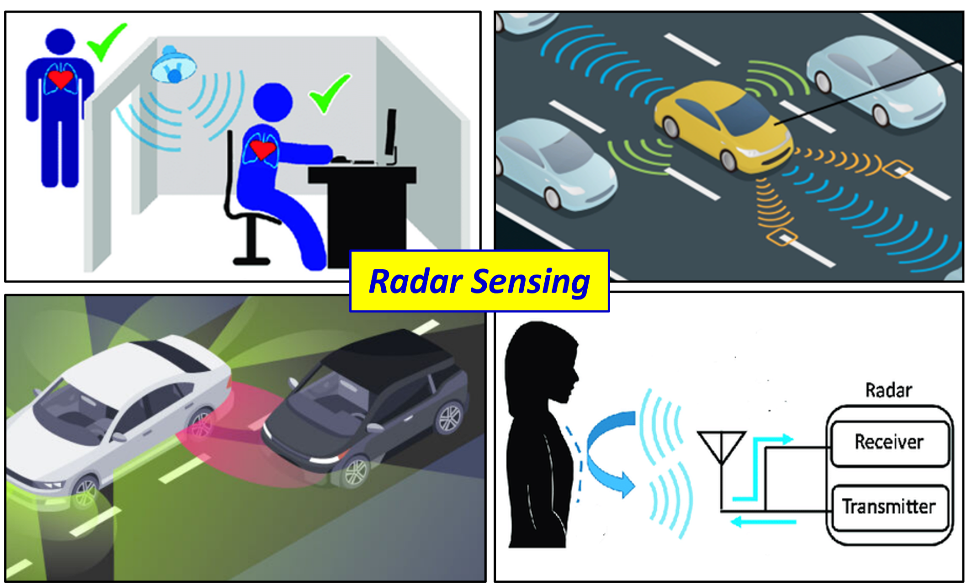

Figure 2.3: FMCW Radar Application areas

2.3.2.0.1 Automotive Cars have evolved beyond mere transportation tools, now emphasizing the enhancement of safety, convenience, and overall driving experience. Modern vehicles offer a range of features, including auto-pilot navigation, streaming media, self-parking capabilities, and voice control for various in-vehicle functions, as highlighted in [3]. Advanced Driver Assistance Systems (ADAS) play a crucial role in this transformation by providing warnings, braking assistance, and steering support for drivers during daily commutes and long-distance road trips, as described in [4]. ADAS technologies have the potential to significantly reduce road accidents by furnishing drivers with enhanced safety features such as blind-spot detection, lane departure warnings, collision alerts, and more. While various sensors contribute to the development of ADAS, FMCW radars are poised to dominate these systems due to their durability, cost-effectiveness, robust performance, and exceptional accuracy.

2.3.2.0.2 Healthcare Vital signs encompass a collection of medical indicators that offer insights into an individual's health status and bodily functions. The fundamental vital signs include heart rate, respiratory rate, blood pressure, and body temperature, as outlined in [5]. Leveraging FMCW (mmWave) radars makes it feasible to achieve precision in object range detection down to millimeter levels, potentially positioning it as an ideal technology for vital sign sensing. Moreover, this technology opens up possibilities for contact-less continuous monitoring of a patient's vital signs, as noted in [6], simplifying the development of large-scale health monitoring systems in healthcare facilities.

Given the advantages and significant potential applications across various domains, it becomes advantageous to invest in the development of the necessary circuitry for FMCW radars. In the upcoming chapter, we delve into the significance of a voltage-controlled oscillator (VCO) within the context of FMCW radar systems along with the design and analysis of a novel VCO topology.

Chapter 3

Design & Analysis of a Voltage Controlled Oscillator (VCO) for FMCW radars operating at mmWave frequency

3.1 Introduction

As discussed previously, FMCW radars emit a frequency modulated wave called chirp. Chirp synthesizer is a key block for FMCW radars responsible for producing low noise chirps with high chirp bandwidth (BW_{ch}) (upto 4 GHz) in short time periods (T_m) ($< 100\ \mu$s). Recently, many Phase Locked Loop (PLL) based chirp synthesizers have been reported for FMCW mmWave radars [7]. Figure 3.1(a), depicts a FMCW chirp synthesizer, where frequency f_0 is synthesized in a PLL using a voltage controlled oscillator (VCO) and multiplied by a factor N to generate 76-81 GHz signal. Direct 76 GHz frequency generation is highly vulnerable to parasitic values, therefore using a multiplier ($N = 2, 3\ or\ 4$) ensures more stability and less phase noise of the 76 GHz band chirp signal. The VCO is the most critical block to generate the mmWave chirp signal with high fidelity.

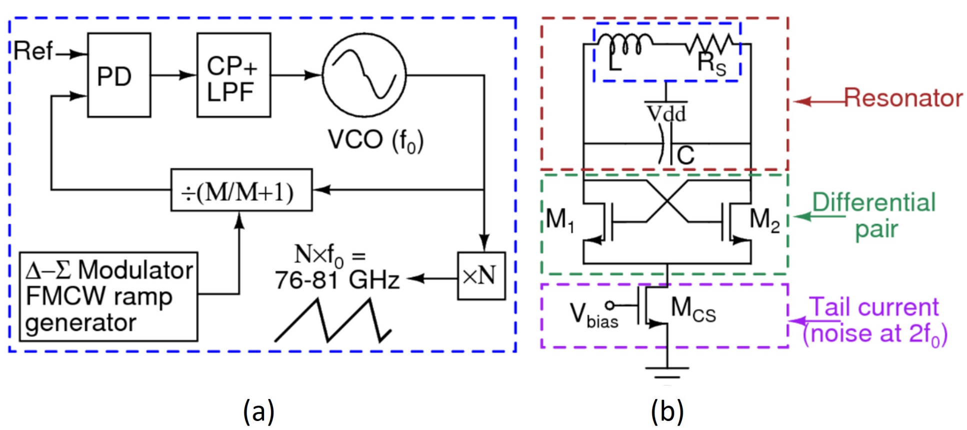

Figure 3.1: (a) PLL block diagram for chirp generation (b) Noise Sources in LC-VCOs

Figure 3.1(b) depicts a conventional cross coupled LC oscillator topology with the major noise sources, which can not directly meet the stringent phase noise requirements at mmWave (>10 GHz) [8], [9]. Towards the goal of building low phase noise VCOs for FMCW chirp synthesizers, in this chapter, we present

- a detailed analysis of an mmWave VCO topology with coupled transformer tank load
- a low phase noise VCO topology for 18.98-20.46 GHz frequency range
- implementation of proposed VCO in 65 nm CMOS technology
- post layout simulation results to validate the proposed low phase noise mmWave VCO topology

3.2 Low Phase Noise VCO Design Techniques

Phase noise ($\mathcal{L}\{\Delta f\}$) of an LC VCO at an offset Δf can be given by Eq. (3.1) [10]

$$\mathcal{L}\{\Delta f\} = F\frac{4kTR}{V_{OSC}^2}\left(\frac{f_0}{2Q\Delta f}\right)^2 \tag{3.1}$$

where, f_0 is the VCO frequency, F is the noise factor of oscillator, defined as the total oscillator phase noise normalized to phase noise due to the LC tank loss (R_s), k is the Boltzmann's constant, T is the temperature in Kelvin, Q is the tank's quality factor and V_{OSC} is the oscillation amplitude.

As depicted in Figure 3.1(b), considering the three main noise sources - 1) resonator tank, 2) the differential pair and 3) the tail current source [11], F of LC oscillators is given by Eq. (3.2) [11].

$$F = 1 + \gamma + \frac{\gamma g_{m_{cs}} R_p}{4} \tag{3.2}$$

where $g_{m_{cs}}$ is the transconductance of the tail current source, γ is the body effect coefficient and $R_p = Q^2 R_s$ is the equivalent parallel resistance of the LC tank at resonance. In Eq. (3.2), the second and third terms correspond to the noise contributions of the differential pair and current source, respectively. Interestingly, as described in [11] the noise of tail current source (CS) present at $2f_0$ gets down converted to f_0 and results in PN degradation. Therefore, phase noise is minimized by minimizing F, which can reach to its fundamental minimum value of $F_{min} = 1 + \gamma$ by filtering the $2f_0$ noise of the tail current source [12].

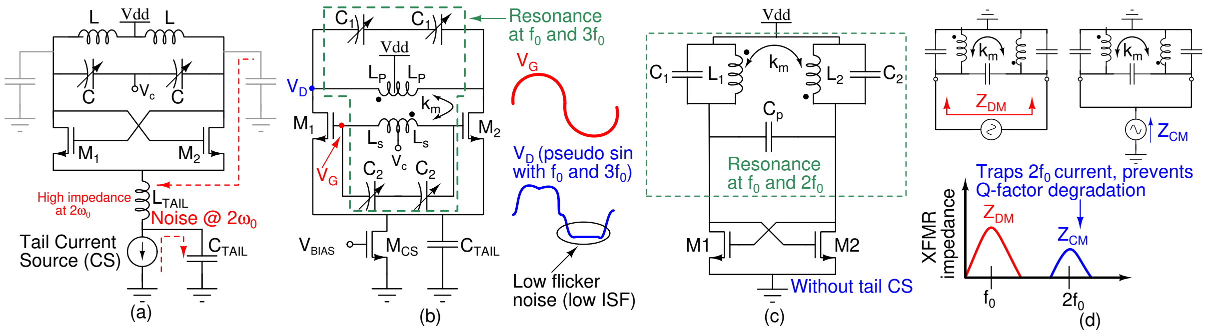

Figure 3.2: (a) CS noise removal using a capacitive filter [12] (b) Use of transformer based VCO for generating sinusoidal and pseudo-sinusoidal waves [13] (c) Topology using implicit common mode impedance (d) DM and CM impedance peaks [14]

Figure 3.2(a) shows the technique presented in [12], where a capacitor (C_{TAIL}) is used in parallel with the CS to filter out $2f_0$ noise component of CS. However, C_{TAIL} also provides a low impedance path to $2f_0$ component of the oscillation signal and degrades the Q factor of the resonator when differential pair transistors move into triode region during oscillation cycles [12]. This happens because the even harmonics ($2f_0,\ 4f_0$, ..) tend to flow through the common mode (CM) path, which exist from resonator to transistors to ground. Fundamental (f_0) and other odd harmonics travel through the differential mode (DM) path, therefore it does not degrade the Q factor of the tank. Therefore, as shown in Figure 3.2(a), an inductor (L_{TAIL}) can be used to provide high impedance to $2f_0$ component of the oscillation signal [12] and prevent Q factor degradation.

However, matching the load and tail tank resonant frequencies is very sensitive to parasitic capacitance, which becomes progressively difficult at higher frequencies. Therefore, implicit CM mode resonance methods have been evolved by utilizing on-chip mutually coupled transformers (XFMR) [13], [14], [15] which can provide more than two resonance modes for improved PN performance.

Figure 3.2(b) depicts a transformer based VCO [13], which has resonant frequencies at 1^{st} and 3^{rd} harmonic in DM. As shown in the figure, a pseudo-sinusoidal wave is generated, which inherently has lower rms value of the impulse sensitivity function (ISF) [16] and hence exhibits reduced phase noise.

Further, as shown in Figure 3.2(c) [14], the tail current source can be removed to avoid $2f_0$ noise down conversion and a transformer can be designed to have impedance peaks Z_{DM} and Z_{CM} at resonant frequencies f_0 and $2f_0$, respectively (Figure 3.2(d)), without requiring any explicit L_{TAIL}. Z_{CM} helps in trapping the 2^{nd} harmonic current in order to reduce the Q-factor degradation from $-g_m$ transistors in triode region thereby reducing the phase noise. However, due to the magnetic flux cancellation, CM Q-factor at $2f_0$ degrades considerably.

To overcome this problem, a CM free topology was proposed in [17], where $2f_0$ resonance in DM was obtained to generate pseudo sinusoidal waveform with lower rms ISF for reduced phase noise. From the preceding discussions, three major approaches emerges to design low phase noise mmWave oscillators:

- to utilize tail current source free topologies with transformer as the load tank
- to utilize CM free topologies to avoid Q-factor degradation and
- to increase Q factor of the tank at $2f_0$ for generating pseudo sinusoidal waveform with low rms ISF. Considering these approaches, we present a transformer based low phase noise, CM free, high-Q VCO design, which is discussed in the next section.

3.3 Proposed VCO Topology & Design Considerations

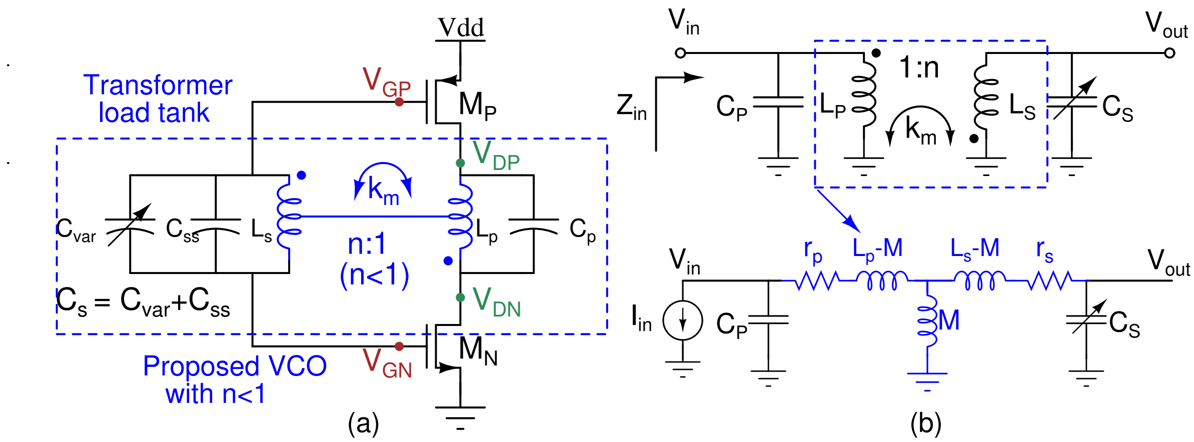

Figure 3.3: (a) Proposed VCO topology with $n < 1$ for mmWave operation (b)Transformer based resonator and its equivalent model

Figure 3.3(a) shows the current reuse VCO topology [17], [18] used in this work, where a transformer with a turn ratio ($n < 1$) has been proposed as the load tank of the VCO. For $1 : n$ multi turn transformer, n can be defined by Eq. (3.3) given below

$$n = k_m \sqrt{\frac{L_s}{L_p}} \tag{3.3}$$

where, L_p, L_s and k_m are the primary-side, secondary-side inductors and coupling coefficient , respectively. As shown in the figure, C_p and C_{ss} are the primary-side and secondary-side fixed metal-insulator-metal (MIM) capacitors, respectively. C_{var} is the varactor used for achieving the desired tuning range. M_P and M_N provides the necessary transconductance to start the oscillations. Figure 3.3(b) shows the electrical equivalent of the transformer [17], [13], where ($C_s = C_{ss} + C_{var}$) is the total capacitance at the secondary-side, ($M = k_m\sqrt{L_pL_s}$) is the mutual inductance, r_p and r_s are the loss resistance of L_p and L_s, respectively. As discussed in section 3.2, for reduced phase noise, pseudo sinusoidal waveform containing f_0 and $2f_0$ components and load tank with high-Q factor near those frequencies are required. Following subsections describe the design considerations for low phase noise mmWave VCO design.

3.3.1 Pseudo sinusoidal waveform and high-Q load tank

3.3.1.0.1 Considerations for pseudo sinusoidal waveform generation As shown in Figure 3.3(b), input impedance (Z_{in}) has a fourth order polynomial denominator resulting in two different resonant frequencies [13]. The lower frequency (f_l) is the operating frequency (f_0) of the VCO, while the higher frequency (f_h) can be a set to the second harmonic ($2f_0$) by adjusting the circuit parameters to achieve pseudo sinusoidal waveform. The ratio $\frac{f_h}{f_l}$ can given by Eq. (3.4) [13],

$$\frac{f_h}{f_l} = \sqrt{\frac{1+\zeta+\sqrt{1+\zeta^2+\zeta(4k_m^2-2)}}{1+\zeta-\sqrt{1+\zeta^2+\zeta(4k_m^2-2)}}} \tag{3.4}$$

where $\zeta = L_sC_s/L_pC_p$.

3.3.1.0.2 Considerations for high-Q load tank To generate multi harmonic (pseudo sinusoidal) voltage waves, high Q impedance at the 1^{st} and 2^{nd} harmonics are used to trap the respective current harmonics. The open loop Q factor of the transformer is given by,

$$Q = \frac{-f}{2} \cdot \frac{d\phi(f)}{df} \tag{3.5}$$

where, $\phi(f) = Z_{in}$. Q factors for the f_0 (Q_1) and $2f_0$ (Q_2) harmonics generated in the tank can be given by Eq. (3.5) and their ratio can be given by Eq. (3.6) [13],

$$\frac{Q_2}{Q_1} = -\frac{1}{4} \cdot \frac{4\zeta^2 - \zeta(1+\frac{Q_S}{Q_P}) + 4\frac{Q_S}{Q_P}}{\zeta^2 - 4\zeta(1+\frac{Q_S}{Q_P}) + 4\frac{Q_S}{Q_P}} \tag{3.6}$$

where Q_s and Q_p are the unloaded Q factors of the secondary and primary sides of transformer, respectively. From Eq. (3.6) we can see that a high ζ and a low $\frac{Q_s}{Q_p}$ helps in achieving a high $\frac{Q_2}{Q_1}$ ratio, which results into pseudo sinusoidal waves at the drain nodes V_{DN} and V_{DP} shown in Figure 3.3(a). As shown in Figure 3.3(b), transformer also provides a passive gain of ($A_v(f)$) defined in Eq. (3.7).

$$A_v(f) = \frac{V_{out}(f)}{V_{in}(f)} = \frac{V_G(f)}{V_D(f)} \tag{3.7}$$

The transformer based resonator shown in Figure 3.3(b) behaves as a biquad filter for $Q_S \times Q_P >> 1$, which results in high A_v for 1^{st} harmonic and low A_v for 2^{nd} harmonic [19]. Therefore, the 1^{st} harmonic of the drain node voltage is amplified and 2^{nd} harmonic is attenuated by the transformer resulting in pure sinusoids with low phase noise at the gate nodes, thus improving the phase noise.

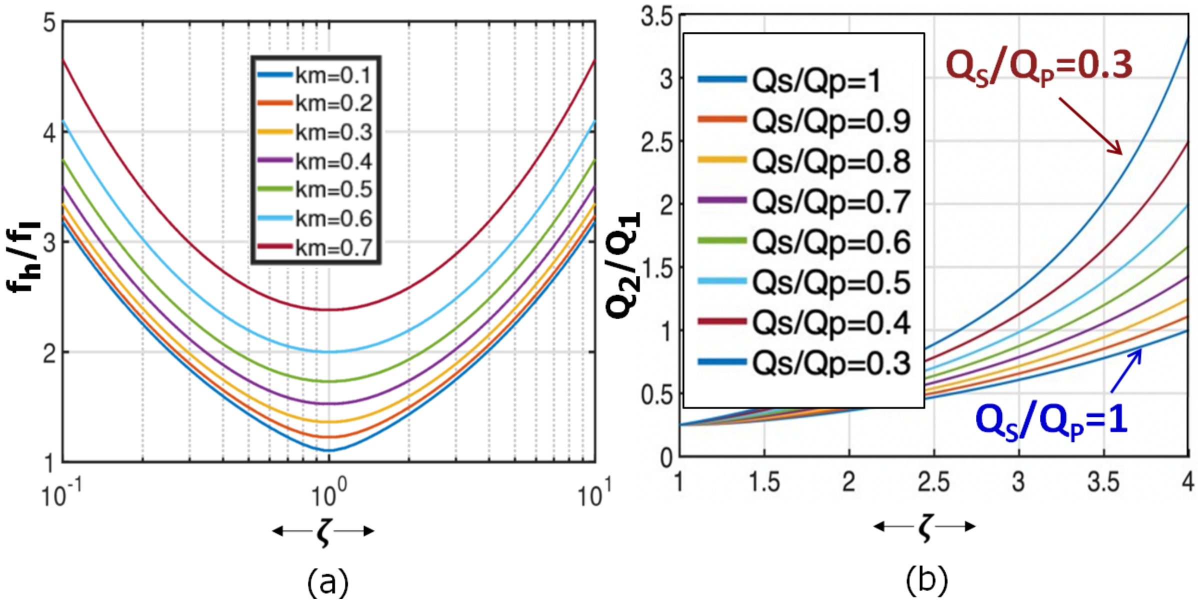

Figure 3.4: (a) f_h/f_l vs ζ for different k_m values (b) Q_{2f_0}/Q_{f_0} vs ζ for different Q_s/Q_p values

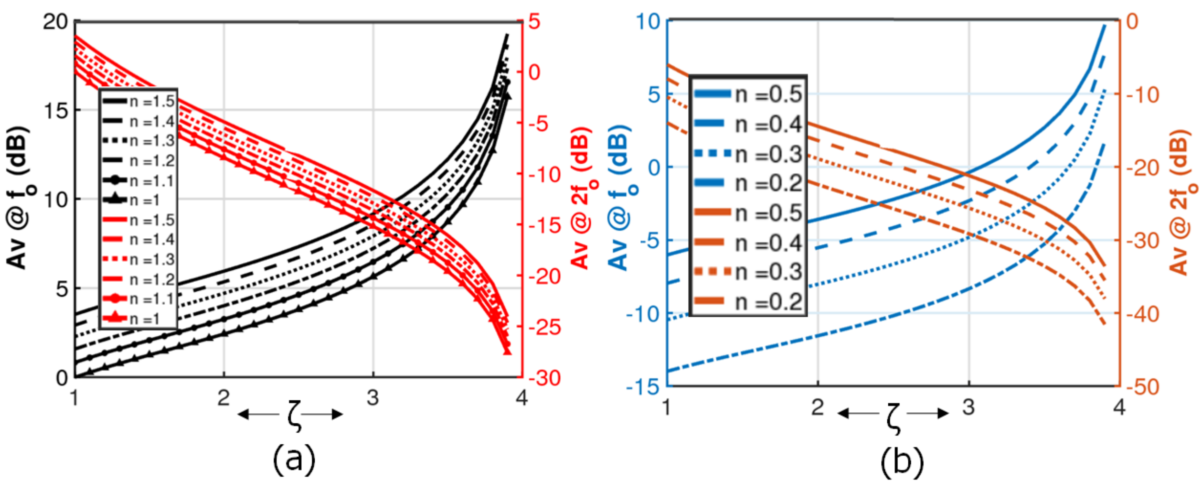

Figure 3.5: Gain vs ζ for first and second harmonics for (a) $n > 1$ (b) $n < 1$

3.3.2 Transformer Design

For the proposed design shown in Figure 3.3(a), to generate pseudo sinusoidal waveform with low rms ISF value, f_h is matched to the second harmonic of the oscillating frequency (i.e. $f_h/f_l = 2$) (Eq. (3.4)).

Figure 3.4(a) shows the plots for $f_h/f_l = 2$ (Eq. (3.4)) for different values of k_m, where $f_l = 20$ GHz and $f_h = 40$ GHz. As shown in the figure, for $f_h/f_l = 2$, $k_m <= 0.6$. At $k_m = 0.6$ we get $\zeta = 1$. From 3.4(b) we can see that at $\zeta = 1$ the $\frac{Q_2}{Q_1}$ ratio is very poor irrespective of $\frac{Q_s}{Q_p}$ ratio.

Eq. (3.6) is plotted in Figure 3.4(b) for ζ values with varying $\frac{Q_s}{Q_p}$ ratios. The Q_s and Q_p values were limited such that the $\frac{Q_s}{Q_p}$ ratio falls between 0.3 and 1. On-chip transformers with single digit Q_s and Q_p values give poor phase noise performance as 1^{st} harmonic starts degrading thereby increasing the effect of thermal noise and degrading phase noise. So assuming $Q_s = 10$ we see that $Q_p = 33.33$ for $\frac{Q_s}{Q_p} = 0.3$. For smaller $\frac{Q_s}{Q_p}$ ratio Q_p values would be too high to be practically realisable. Beyond $\frac{Q_s}{Q_p} = 1$ it is not possible to get high $\frac{Q_2}{Q_1}$ ratio as can be seen from Figure 3.4(b). Therefore to achieve a high $\frac{Q_2}{Q_1}$ ratio for $\frac{Q_s}{Q_p}$ between 1 and 0.3 ζ should be considerably higher than 1 (preferably > 3). Consequently for ζ values > 3 we have to choose a lower k_m value from Figure 3.4(a). Substituting $k_m = 0.3$ and $n = 1$ in Eq. (3.3) we get, $1 = 0.3\sqrt{\frac{L_s}{L_p}}$, which results in Eq. (3.8).

$$L_s = 11.1 \times L_p \tag{3.8}$$

For comparing the Q-factors of various inductor sizes, simulations were done in ASITIC. Table 3.1 shows Q-factor of different inductor values at 20 GHz. From Table 3.1 we can see that at 20 GHz the best Q factor is achieved by single turn inductors in the range of 350-100 pH. If these inductors are used in designing L_p, then L_s value will be around 3-1 nH according to Eq. (3.8). Such high inductors require multi turn designs that degrade Q factors to a great extent which can have a negative effect on the phase noise. Taking values lower than 100 pH for designing the primary inductor will also result in degraded Q factor. Therefore, we propose that the $1 : n$ transformer based VCO requires turns ratio $n < 1$ to function in mmWave region with good phase noise performance. Only then the inductors on the primary and secondary side would fall in the 350-100 pH with comparable Q factors. The drawback for $n < 1$ turns ratio is that voltage gain for 1^{st} harmonic would be low (Figure 3.5(b)) unlike in the case of $n > 1$ (Figure 3.5(a)). But this is already remedied when a higher ζ value is chosen ensuring sufficient gain for 1^{st} harmonic.

Once the oscillator is designed using this transformer based resonator it has to achieve the target tuning range. The following subsection discusses the tuning range technique and its effect on the phase noise performance on the VCO.

Table 3.1: Quality factor Comparison for Multi & Single Turn Inductors at 20 GHz by using ASITIC

Outer Radius (μm)	100	100	100	50	50	50	30	30
No. of Turns	3	2	1	2	1	1	2	1
Width of Metal	20	20	20	10	10	20	7	15
Turn Spacing (μm)	10	10	10	5	5	5	5	5
Inductance (nH)	1.13	0.83	0.34	0.44	0.174	0.126	0.2	0.071
Quality Factor	7.15	14.12	35.84	33.66	35.78	45.82	31.88	38.21

3.3.3 Tuning range

For tuning the proposed VCO varactors were placed parallel to the existing metal-insulator-metal (MIM) capacitor (very high Q factor) on the secondary side of the resonator tank. This would reduce the overall Q factor of the secondary side (Q_s = 11) while preserving the Q factor on the primary side (Q_p = 28) ensuring a low $\frac{Q_s}{Q_p}$ and improving the $\frac{Q_2}{Q_1}$ ratio for $\zeta = 3.771$ as shown in Figure 3.4(b). A drawback of this method is that upon tuning the varactor the net capacitance on the secondary side C_s changes thus changing ζ which changes $\frac{Q_2}{Q_1}$ ratio of the VCO tank as can be seen from Eq. (3.6). This will make it difficult to match impedance peaks exactly at the 1^{st} and 2^{nd} harmonics (i.e $\omega_h/\omega_l \neq 2$). Consequently, a high $\frac{Q_2}{Q_1}$ ratio is not guaranteed throughout the tuning range allowing flicker noise up-conversion thereby degrading phase noise performance when the VCO is being tuned. Even though the target tuning range is achieved, there will be minor phase noise performance degradation as the VCO is tuned.

3.4 Implementation & Simulation Results

This section presents the implementation details and simulation results of the proposed custom-designed transformer and complete VCO in 65nm CMOS process. Taking into consideration the parameters discussed in Section 3.3.2, the transformer has been designed in ASITIC and further optimized in HFSS to obtain high Q factor in the mmWave frequency range.

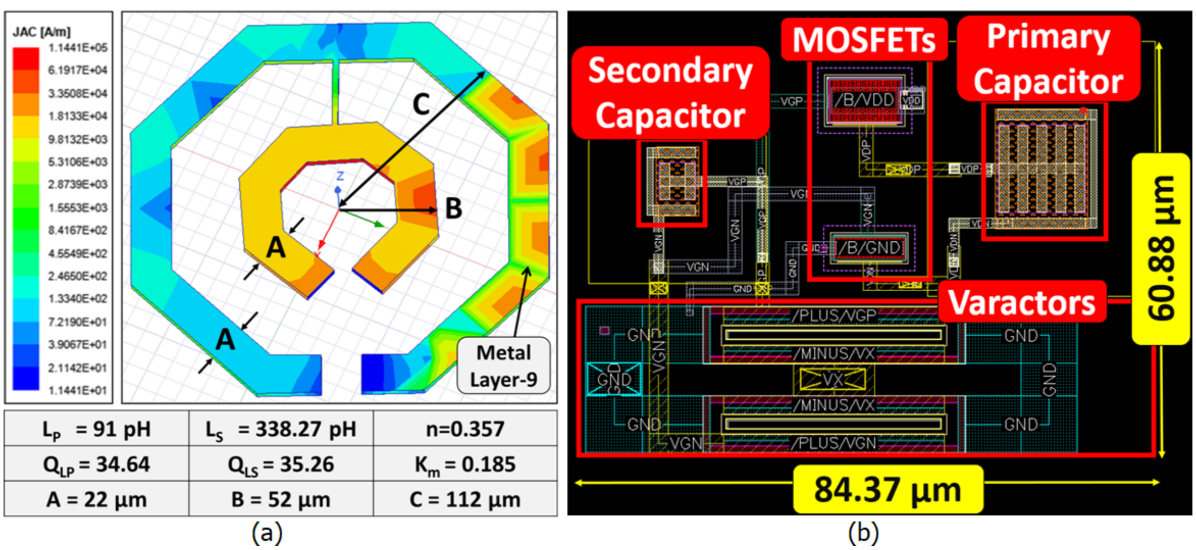

Figure 3.6: (a) Specifications of custom-designed transformer with $n < 1$ in HFSS (b) Layout in 65 nm CMOS technology (TSMC) of the proposed design

As shown in Figure 3.6(a), the designed transformer has L_p = 91 pH and L_s = 338.27 pH with high Q factors to ensure good phase noise performance. Schematic and post-layout simulations been carried out using the S-parameter file generated by HFSS. Figure 3.6(b) shows the proposed VCO implementation in 65nm CMOS process. The proposed VCO in schematic simulations consumes 12.52 mA of current from a 1.1 V supply.

Figure 3.7(a) shows the phase and magnitude plots of the transformer's trans-impedance with $Q_1 = 11.64$ and $Q_2 = 17.73$. The significant $\frac{Q_2}{Q_1}$ ratio ensures improved phase noise performance. Figure 3.7(b) shows the magnitude plots of the transformer's trans-impedance across the tuning range. Figure 3.7(c) shows the transient waveforms obtained at each of primary and secondary coil nodes in the design. V_{DN} and V_{DP} are pseudo-sinusoidal in nature while V_{GN} and V_{GP} are composed of the 1^{st} and 2^{nd} harmonics of the drain node voltages which are amplified and compressed, respectively, by the transformer's passive gain resulting in sinusoidal voltages. The phase and amplitude mismatches between the 2 terminals obtained as a result of parasitics can be rectified in order to facilitate differential outputs by optimizing transistor sizing to ensure matching of harmonic peaks.

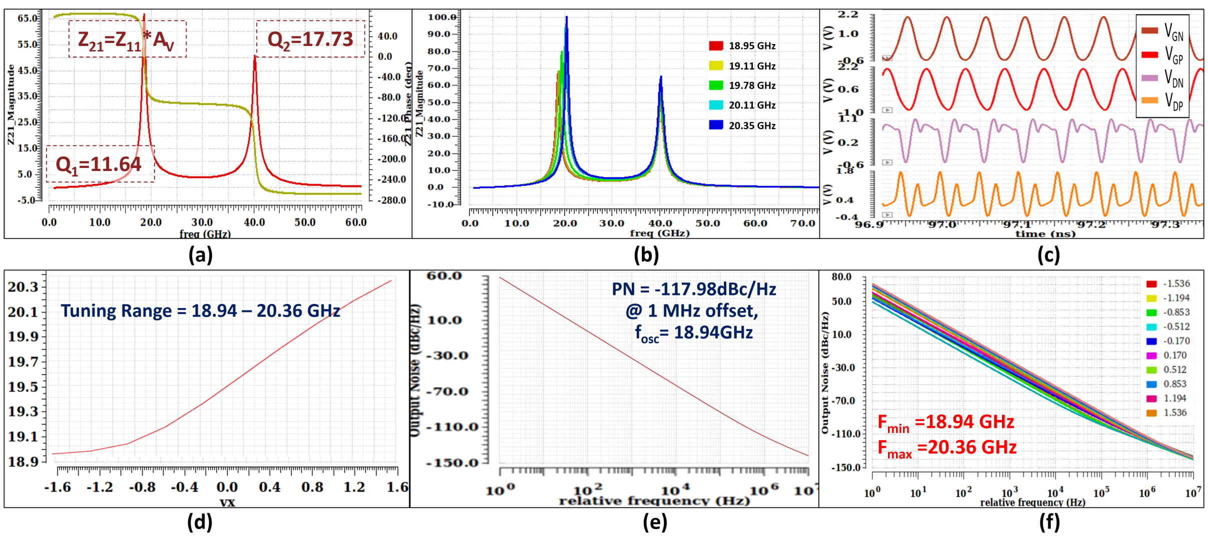

Figure 3.7: Post layout simulation results showing (a) phase and magnitude values of transformer's trans-impedance with Q_2 and Q_1 values (b) magnitude values of transformer's trans-impedance throughout the tuning range (c) transient waveform showing pseudo sinusoid behaviour at drain nodes and pure sinusoid at gate nodes (d) tuning range (e) phase noise (f) phase noise over the tuning range

As shown in Figure 3.7(d), the tuning range of the VCO is 1.42 GHz (18.94 - 20.36 GHz) in post-layout simulations as compared to 1.48 GHz (20.48 - 21.96 GHz) in schematic simulations. There is a decrease in operating frequency due to the presence of parasitic capacitances which can be associated with the improvement in phase noise performance from -115.36 dBc/Hz at 1 MHz offset from 20.48 GHz in schematic simulations to -117.98 dBc/Hz at 1 MHz offset from 18.94 GHz in post-layout simulations. Figure 3.7(e) shows the phase noise performance of the implemented VCO to be -117.98 dBc/Hz at a 1 MHz offset from the oscillation frequency of 18.94 GHz. As shown in Figure 3.7(f), the VCO phase noise performance is greatly improved in the mmWave frequency range due to a high $\frac{Q_2}{Q_1}$ ratio with $PN = -117.98$ dBc/Hz at $f_{osc} = 18.94$ GHz and $FoM = 192.13$ dB. While tuning the VCO we change C_{var} due to which there will be a frequency mismatch between the 1^{st} and 2^{nd} harmonic impedance peaks as opposed to the matched peaks at 18.94 GHz leading to some flicker noise up-conversion and phase noise degradation as previously discussed in Section 3.3.3.

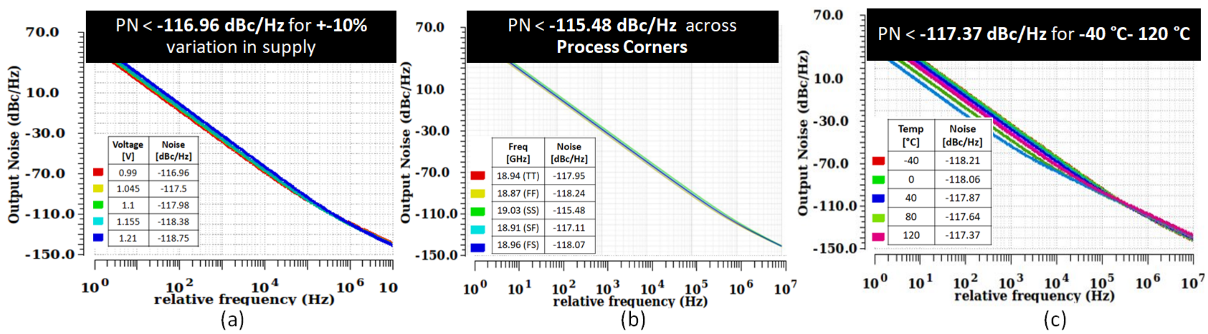

Figure 3.8: Post layout phase noise variation at 1 MHz offset with variations in (a) supply voltage (b) process corners (c) temperature

Table 3.2: Performance Summary and Comparison with State of the Art

Parameters	**[20]**	**[21]**	**[22]**	**[23]**	**[24]**	**[25]**	**[26](This Work)**
Measured/Simulated	Measured	Measured	Measured	Measured	Measured	Measured	Simulated
Technology	65 nm CMOS	65 nm CMOS	65 nm CMOS	180 nm CMOS	22 nm FD-SOI	65 nm CMOS	65 nm CMOS
Supply Voltage (V)	0.48	1	1	NA	0.8	0.6	1.1
Frequency (GHz)	25.48-29.92	24.62-28.66	20.7-28	17.5	24.9	25	18.94-20.36
Power Consumption (mW)	4	9.7-10.5	12.65-15.12	2.3	8.8	4.8	13.78
Area (mm*mm)	0.32*0.25	0.52*0.37	0.24*0.47	0.56*0.18	0.043mm^2	0.13*0.9	0.084*0.060(Active Circuit) 0.0605mm^2(Transformer)
Phase Noise at 1MHz offset (dBc/Hz)†	-115.27	-111.4	-107.9	-110.77	-110.2	-110	-117.98
FoM (dBc/Hz) $^{\dagger\diamond}$	191.6	189.4	184.75	191.95	188.6	191.2	192.13

†Estimated from plots

$$^{\diamond}FoM = -PN + 20log_{10}(f_{lo}/\Delta f) - 10log_{10}(P_{DC}/1mW)$$

As shown in Figure 3.8, the deviation in phase noise performance is 1.79 dBc/Hz for a $\pm$ 10 % variation in supply voltage and 2.76 dBc/Hz across process corners with phase noise < -115.48 dBc/Hz at an offset of 1 MHz for all corners. Phase noise performance is also consistent across temperatures emphasizing the robustness of the proposed VCO with values < -117.37 dBc/Hz at 1 MHz offset for temperatures ranging from -40°C to 120°C. Table 3.2 presents the performance summary of the proposed design and its comparison with other recently reported works. As shown in the table, the post layout simulation results of the proposed design shows promise as compared to the other works with measurement results. The proposed VCO exhibits a better phase noise performance and FoM, while making use of a simple single coil inductor topology along with a simple tuning technique as opposed to complex multi-coil topologies with tuning techniques involving switching between modes of operation used in other recent works.

In this chapter, design and analysis of a low phase noise, transformer tank based mmWave voltage controlled oscillator (VCO) near 20 GHz has been presented. The proposed VCO is designed for multiplier based 77 GHz FMCW chirp synthesizers. The following chapter deals with the design and analysis of a VCO operating in mmWave region inspired from the Colpitts Oscillator.

Chapter 4

Design and Analysis of 20 GHz VCO based on Colpitts Topology

4.1 Introduction

CMOS technology offers reduced cost and high level of integration for transceivers. It is extensively used for designing various circuit components like voltage controlled oscillator (VCO), mixer, frequency divider, low-noise amplifier (LNA). VCOs are a critical part of transceiver systems. Designing low power and low phase noise VCOs at mmWave frequencies are a challenge for designers due to the naturally high flicker noise of MOSFETs. Cross-coupled VCOs are favored for their simple design, differential operation, and lenient start-up requirements. Nonetheless, this configuration experiences considerable degradation in phase noise as a result of the noise generated by the active components when the oscillator becomes highly vulnerable to disturbances [16]. In contrast, the Colpitts oscillator is capable of better performance phase noise wise as it is more resistant to cyclostationary noise [16]. This could be greatly advantageous for oscillator design in mmWave region, improving overall transceiver performance. However, they are seldom utilized in integrated transceivers due to their high gain requirement for attaining a stable start-up, leading to increased power consumption in comparison to cross-coupled oscillators. In this chapter, we present a novel VCO based on the Colpitts topology with low power consumption and low phase noise resulting in high figure of merit (FOM) for mmWave applications.

4.2 The evolution of Colpitts oscillator

The single sideband phase noise ($\mathcal{L}\{\Delta\omega\}$) of an oscillator in the $1/f^2$ region is defined as [16],

$$\mathcal{L}\{\Delta\omega\} = \frac{\bar{i_n^2}/\Delta f}{2q_{max}^2}\left(\frac{\Gamma_{eff,rms}^2}{\Delta\omega^2}\right) \tag{4.1}$$

where $\Delta\omega$ is the carrier offset frequency, $\bar{i_n^2}/\Delta f$ is the power spectral density of the current noise source of interest, $\Gamma_{eff,rms}^2$ is the RMS value of the effective impulse sensitivity function (ISF) of that noise source, and q_{max} is the maximum charge swing across the current noise source. Effective ISF is defined as the product of ISF and noise modulating function (NMF) [16], [27],

$$\Gamma_{eff}(\omega t) = \Gamma(\omega t) \cdot \alpha(\omega t) \tag{4.2}$$

where $\Gamma(\omega t)$ is the ISF representing the time-dependent sensitivity of the oscillator's phase to disturbances and $\alpha(\omega t)$ denotes the NMF that explains the modulation of the noise power spectrum with time for the noise source of interest. From equation (4.1) it can be concluded that $\Gamma^2_{eff,rms}$ should be as low as possible to reduce phase noise.

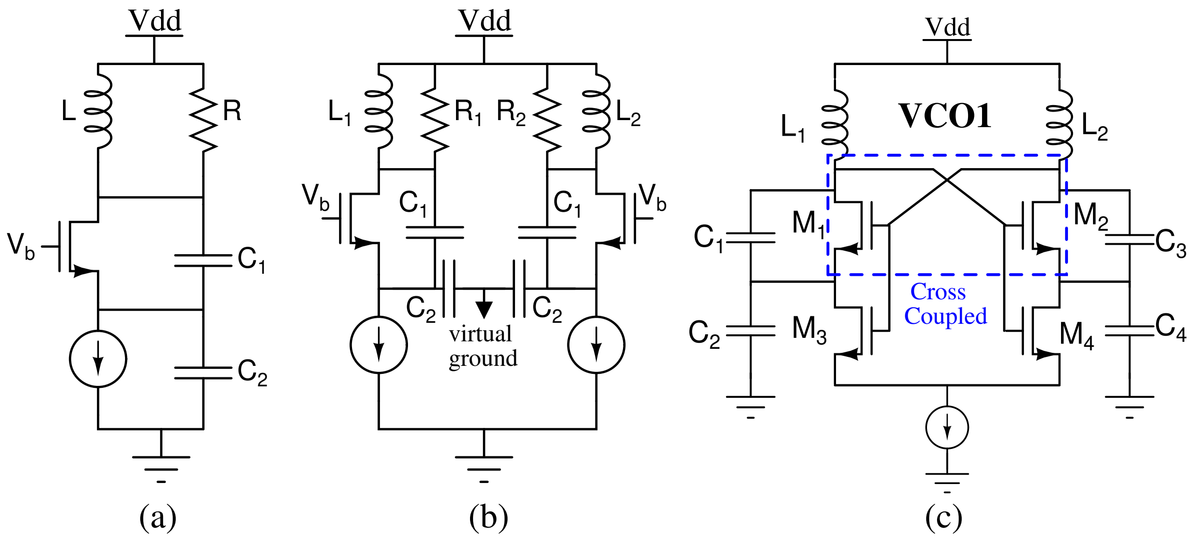

Figure 4.1: (a) Colpitts oscillator (b) differential Colpitts oscillator [28](c) cross-coupled Colpitts oscillator [29]

In [28] it was demonstrated that the single-ended Colpitts oscillator, depicted in Fig. 4.1(a), had a smaller RMS and dc value of its effective ISF compared to both NMOS-only and complementary cross-coupled oscillators. This was achieved through simulation of $\Gamma(\omega t)$, $\alpha(\omega t)$, and $\Gamma_{eff}(\omega t)$ which revealed that the moment of highest noise generation (highest NMF) coincided with the oscillator's least sensitive point (lowest ISF), implying a potential reduction in phase noise. Hence, single ended Colpitts oscillator has superior immunity to cyclostationary noise compared to the cross-coupled topologies. However, the single-ended nature of Colpitts oscillators make them more prone to common-mode noise sources. To address this issue, a differential Colpitts oscillator was designed in [28] by combining two identical Colpitts oscillators, as shown in Fig. 4.1(b). The central node, where the C_2 capacitors are connected, serves as a floating differential virtual ground for proper operation. This topology retained the cyclostationary noise-shaping advantages provided by the core transistors' behavior which would be beneficial for oscillators operating in the mmWave region. A notable disadvantage of this configuration is the increase in power consumption by a factor of 2 under similar start-up conditions.

In [29], a cross-coupled Colpitts oscillator was proposed as a solution to the previously mentioned problem. As shown in Fig. 4.1(c) (**VCO1**), M_1 and M_2 are cross-coupled, resulting in a self biased oscillator. To find the small signal admittance of this VCO, we look into the drain of either M_1 or M_2 [29],

$$Y_{in} = \frac{S^2C_1C_2 - g_mSC_2}{g_m + S(C_1 + C_c)} \tag{4.3}$$

The real part is given by,

$$Re[Y_{in}] = -\frac{g_m\omega^2C_2[2C_1 + C_2]}{g_m^2 + \omega^2(C_1 + C_2)^2} \tag{4.4}$$

The real part of negative small signal admittance for a conventional Colpitts oscillator is given by,

$$Re[Y_{in}] = -\frac{g_m\omega^2C_1C_2}{g_m^2 + \omega^2(C_1 + C_2)^2} \tag{4.5}$$

By examining equations (4.4) and (4.5), it becomes apparent that the negative admittance produced in VCO1 is amplified by a factor of $2 + \frac{C_2}{C_1}$ relative to the traditional Colpitts oscillator. As a result, the power required to achieve a stable start-up is decreased [29]. We introduce a novel 20 GHz Colpitts VCO, which exhibits reduced power consumption compared to VCO1, while maintaining similar phase noise performance making it suitable for integration into transceivers.

4.3 Proposed VCO Topology

4.3.1 Power Reduction

As illustrated in Fig. 4.2(a) (**VCO2**), a cross-coupled PMOS network is introduced to the existing topology of VCO1. Subsequently, the net g_m of the new topology (VCO2) increased allowing reduced current consumption. Table 4.1, that compares schematic simulation results of VCO1, VCO2, and VCO3 under same conditions, shows that the addition of the cross-coupled PMOS resulted in a 46% reduction in power consumption. Understandably, the addition of M5 and M6 to the circuit adversely affects the phase noise, compared to VCO1. As shown in Table 4.1, the phase noise degrades by 12 dB. Remedial measures taken to improve the phase noise performance are discussed in the following subsection.

Table 4.1: Performance Comparison of VCO1, VCO2, VCO3 Based on Schematic Simulations in 65nm CMOS

Parameter	**VCO1**	**VCO2**	**VCO3 (coupling coeff = 0.4)**
Frequency (GHz)	19.82	19.84	19.87
Inductor Q factor	20	20	20
VDD	1	1	1
Power Consumption (mW)	1.5	0.8	0.8
Phase Noise (dBc/Hz)	112.67	99.05	112.52
FoM (dBc/Hz)	196.85	185.96	199.45

$$FoM = -PN + 20log_{10}(f_{lo}/\Delta f) - 10log_{10}(P_{DC}/1mW)$$

4.3.2 Phase Noise Improvement

As discussed in section 4.2, the key to reducing phase noise is to reduce Γ_{eff}. This can be done through generation of pulse like (pseudo-sinusoidal) voltage waveforms. Such waveforms have inherently RMS value of the impulse sensitivity function (ISF) leading to a reduction in phase noise [16]. As shown in Fig. 4.2(b), the fundamental concept underlying the generation of a pseudo-sinusoidal wave involves capturing current harmonics. In a typical LC-tank oscillator the drain current is generally a square wave, comprising both fundamental and higher harmonic components. However, the tank's input impedance only exhibits a magnitude peak at the fundamental frequency, effectively filtering out the higher harmonic components of the drain current and yielding a sinusoidal wave across the tank. If the tank were to provide additional input impedance magnitude peaks at higher harmonics of the fundamental frequency, the respective current harmonics would not be filtered out. As a result, the oscillation voltage would contain a significant amount of the higher harmonic component, in addition to the fundamental harmonic. This would generate a pseudo-sinusoidal wave as illustrated in Fig. 4.2(b). A resonator tank with multiple impedance peaks can be synthesized using a transformer. Several works have utilized this technique for phase noise reduction [13] [15], [17], [26]. For the above mentioned reasons, in this work (**VCO3**) a transformer-based resonator tank is used, as shown in Fig. 4.2(c). Compared to VCO2, the phase noise in VCO3 improved by 12 dB, as presented in Table 4.1. The following section discusses the implementation and post layout simulation results of the proposed topology.

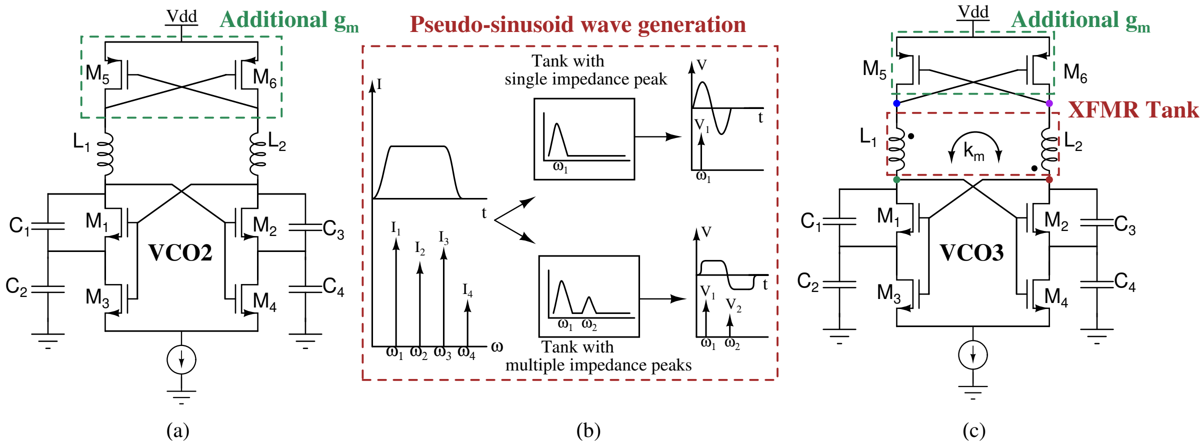

Figure 4.2: (a) Introduction of PMOS cross-coupled structure for power reduction (b) pseudo-sinusoidal wave generation (c) proposed VCO topology

4.4 Implementation & Post Layout Simulation Results

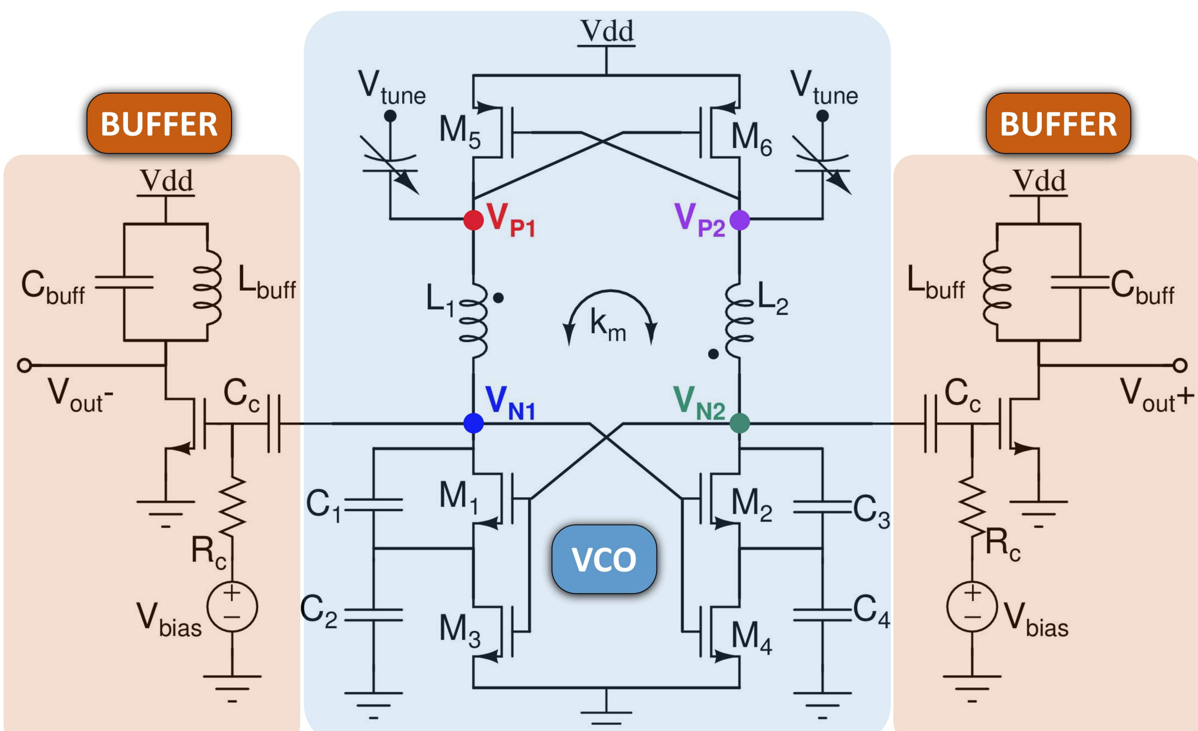

Figure 4.3: Proposed VCO with varactors and LC tuned buffer

Fig. 4.3 shows the final implemented design of the proposed VCO topology in TSMC 65nm. As demonstrated in Fig. 4.3, there is no current bias used in this particular VCO design. This provides more voltage headroom for the other MOSFETs in the design and eliminates a potential source of noise. Additionally, varactors are incorporated for tuning the VCO. Buffers are designed such that the output of the VCO output remains stable across the tuning range.

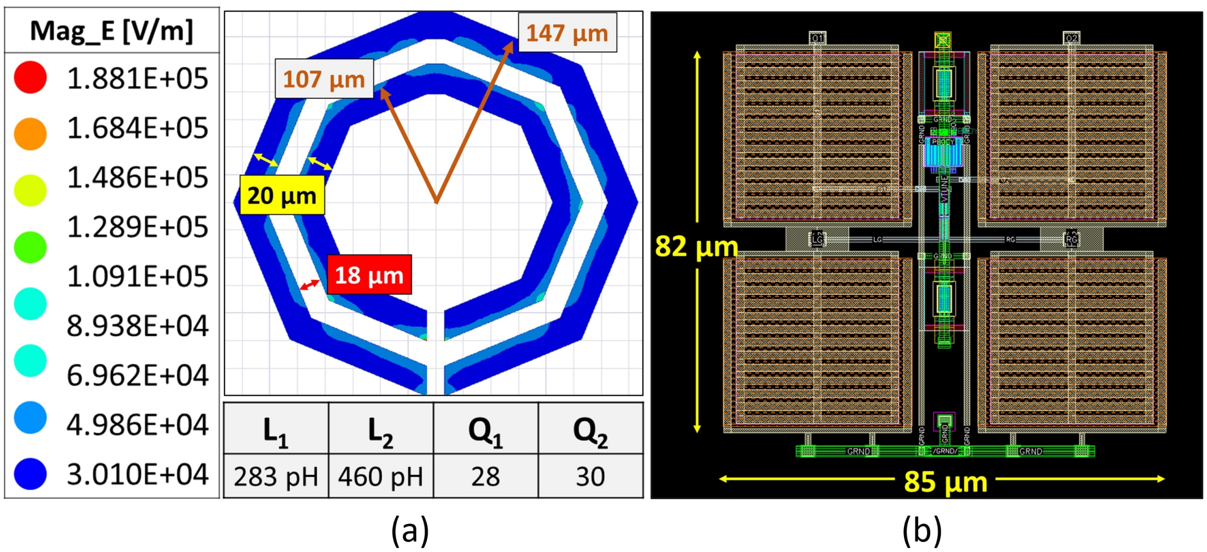

Figure 4.4: (a) Custom-designed transformer in HFSS (b) layout of the proposed VCO in 65 nm CMOS technology (TSMC)

4.4.1 Transformer Design Implementation

The on-chip transformer (XFMR) is designed using ASITIC and optimized in HFSS to achieve high Q-factors at mmWave frequencies [26]. As depicted in Fig. 4.4(a), the designed XFMR covers an area of 294 μm×294 μm with L_1 = 283 pH and L_2 = 460 pH. The primary and secondary coils of the XFMR have high Q factors with Q_1 = 28 and Q_2 = 30, ensuring good phase noise performance.

4.4.2 Post Layout Results

Fig. 4.4(b) shows the layout of the proposed VCO in TSMC 65nm other than the XFMR. The VCO core along with the capacitors and varactors cover an area of 82 μm×85 μm. Post-layout simulations were done in SpectreRF using the S-parameter file created via HFSS. The designed VCO draws a current of 1.2 mA from a 1 V supply. Fig. 4.5(a) and Fig. 4.5(b) depict the transient waveforms obtained at the nodes V_{P1}, V_{N1}, V_{OUT-} and V_{P2}, V_{N2}, V_{OUT+} respectively. Fig. 4.5(c) shows the DFT plots for V_{P1} and V_{N1} that confirms the presence of higher order harmonics in the output voltage waveforms. The buffers driven by the VCO completely filter out the higher harmonics resulting in just the fundamental harmonic as shown in the DFT plot for V_{OUT-}. Fig. 4.5(d) and Fig. 4.5(e), depict the perturbation projection vector (PPV) plots [30] obtained at V_{P1}, V_{P2} and at V_{N1}, V_{N2} respectively. The PPV plots for V_{P1} and V_{P2} have flat regions with $\Gamma_{PPV}(t) = 0$ due to the pseudo-sinusoidal nature of the corresponding voltage waveforms. As a result, Γ_{eff} reduces resulting in low phase noise as discussed previously in section 4.2.

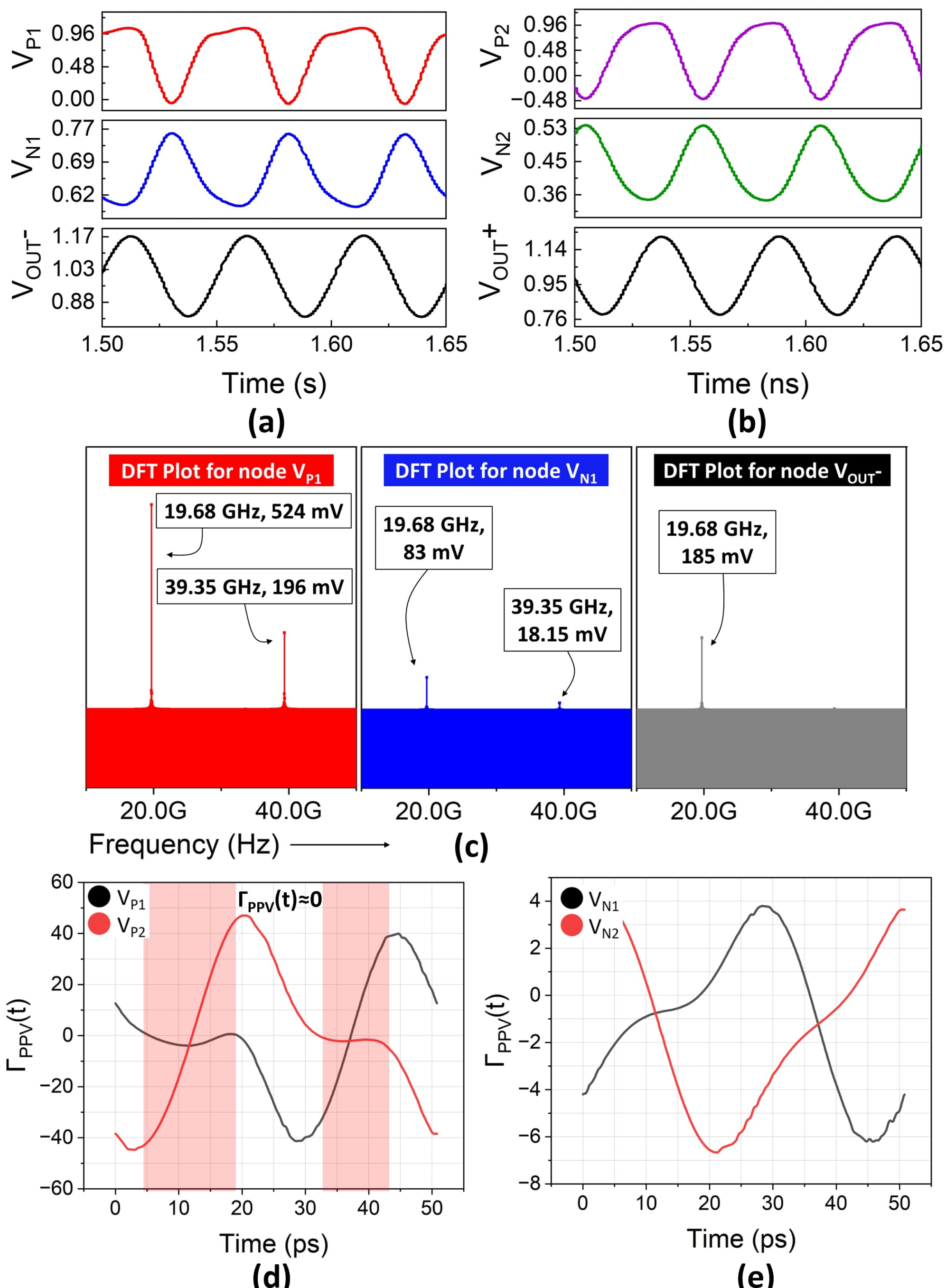

Figure 4.5: (a) Transient waveforms for V_{P1}, V_{N1}, and V_{OUT-} (b) transient waveforms for V_{P2}, V_{P2}, and V_{OUT+} (c) DFT plots for V_{P1}, V_{N1}, and V_{OUT-} (d) PPV plots for V_{P1} and V_{P2} (e) PPV plots for V_{N1} and V_{N2}

Fig. 4.6(a) shows the VCO's tuning range of 1.7 GHz (18 - 19.7 GHz) while Fig. 4.6(b) shows that VCO phase noise is <-100.26 dBc/Hz across the tuning range. Fig. 4.6(c) demonstrates consistent phase noise performance of the VCO across temperatures (<-109.25 dBc/Hz at 1 MHz offset) from -40°C to 120°C. Fig. 6(d) depicts that a ±10% variation in supply voltage results in a 1.969 dBc/Hz deviation in phase noise, while Fig. 6(e) shows the corresponding deviation in oscillating frequency. Fig. 6(f) illustrates a phase noise deviation of 2.211 dBc/Hz across process corners, with phase noise <-110.235 dBc/Hz at a 1 MHz offset for all corners. Fig. 6(g) and Fig. 6(h) depict the effects of ±10% variation in coupling coefficient and quality factor, respectively, on phase noise. Table 4.2 provides a concise overview of the performance of the proposed VCO topology, including a comparative analysis with recently published works. The table illustrates that the post layout simulation results of the proposed VCO exhibit encouraging performance in comparison to other measured and simulated studies. Specifically, the proposed VCO stands out for its lowest power consumption, good phase noise performance, and superior FoM.

This chapter discusses a novel g_m-boosted Colpitts VCO designed in CMOS TSMC 65 nm technology using a transformer based resonator tank. Detailed post-layout simulation results and analysis of the VCO demonstrate a figure-of-merit of 196.26 dBc/Hz and a phase noise of -111.21 dBc/Hz at a 1 MHz offset when operating at 19.6 GHz. Additionally, the VCO achieves a tuning range of 1.7 GHz (18-19.7 GHz) while consuming a power of 1.2 mW from a 1 V supply.

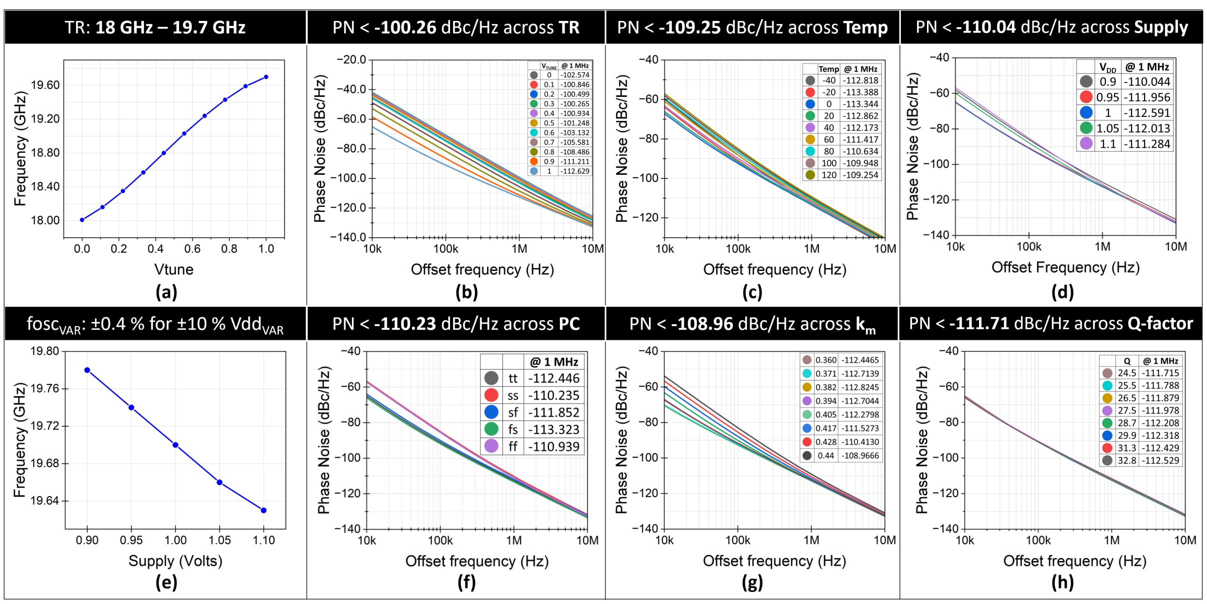

Figure 4.6: Post Layout simulations showing (a) tuning range (b) variation in phase noise across TR (c) variation in phase noise with temperature (d) variation in phase noise with supply (e) frequency variation with supply voltage (f) variation in phase noise across process corners (g) variation in phase noise with coupling coefficient (h) variation in phase noise with quality factor of L_2

Table 4.2: Post Layout Performance Summary and Comparison with Prior Works

Attributes	[31]	[32]	[33]	[34]	[35]	[25]	**This Work**
Simulated/Measured	Measured	Measured	Simulated	Simulated	Measured	Measured	Simulated
Technology Node (CMOS)	28 nm	90 nm	65 nm	40 nm	28 nm	65 nm	65 nm
Supply Voltage (V)	0.9	1.15	0.85	-	1.8	0.6	1
Frequency (GHz)	19.5 (12 % TR)	18 - 20.25	2.408 - 2.48	23.4 - 27.6	18.7 (11.6% TR)	25 (12% TR)	18 - 19.7 (9% TR)
Power Consumption (mW)	20.7	8.13	2.38	12.69	90	4.8	1.2
Area	0.07 mm^2	-	0.765 mm^2	0.25 mm×0.64 mm	0.038 mm^2	0.13 mm×0.9 mm	0.082 mm×0.085 mm (Core) 0.0611 mm^2 (Transformer)
Phase Noise at 1MHz offset (dBc/Hz)	-112	-117.34	-117.873	-106.6	-113.8	-110	-111.211
FoM (dBc/Hz) $^\diamond$	185	193.24	181.88	183.1	180	191.2	196.26

$$^\diamond FoM = -PN + 20log_{10}(f_{lo}/\Delta f) - 10log_{10}(P_{DC}/1mW)$$

The following chapter consists of a brief discussion of systems developed using commercially available FMCW radars. These systems are designed for classifying objects and detecting heart and breath rates.

Chapter 5

Design of Measurement Circuit & System Design using FMCW Radars

In this chapter, a concise overview is presented regarding the systems created utilizing FMCW radar technology. The various applications and solutions that have emerged from the utilization of FMCW radar systems is discussed, emphasizing the significance of this technology in diverse contexts.

5.1 Design of Measurement Circuit

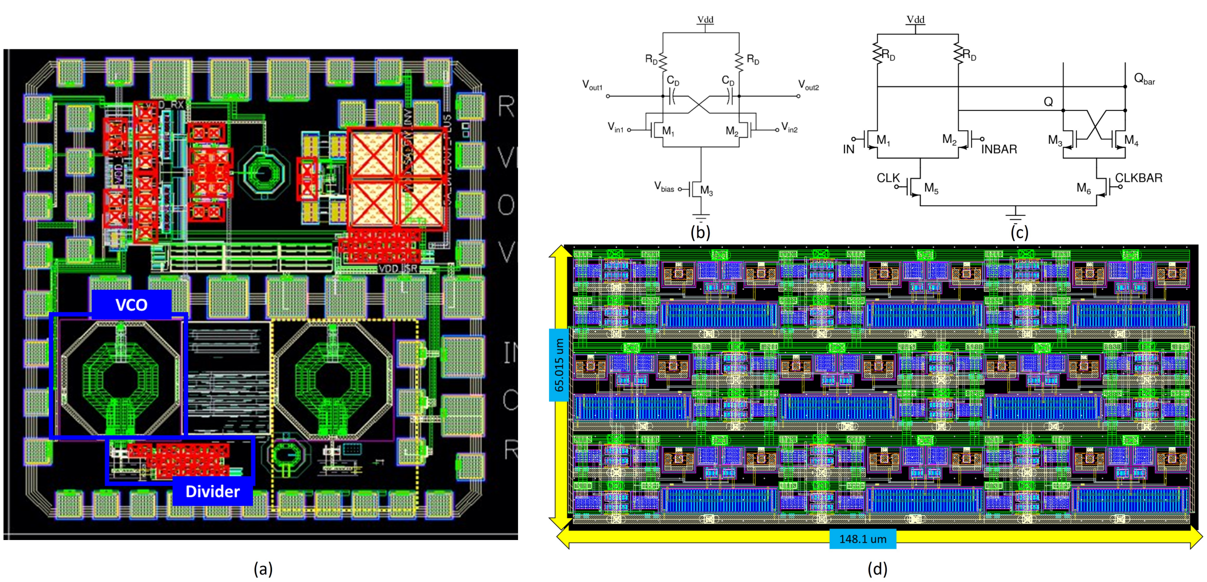

Figure 5.1: (a) Designs for tapeout (b) CML Buffer (c) CML Latch (d) High frequency divider

Figure 5.1(a) shows the designs that have been sent for tapeout by our research group. I contributed towards this tapeout by designing a frequency divider (highlighted in Figure 5.1(a)) that would help measure the output of the VCO (highlighted in Figure 5.1(a)). The divider was designed using current mode logic (CML) and consists of CML buffers and latches and their schematics are presented in Figure 5.1(b). The layout of the entire divide by 512 block is presented in Figure 5.1(c) along with the dimensions. The divider is designed to handle inputs as high as 20 GHz with a supply of 1.2 V with a power consumption of 25 mW. Figure 5.2(a) shows the test bench setup for post layout simulations of the divider. Figure 5.2(b) shows the differential output from the VCO at 20 GHz while Figure 5.2(c) shows the final divided output at 40 MHz.

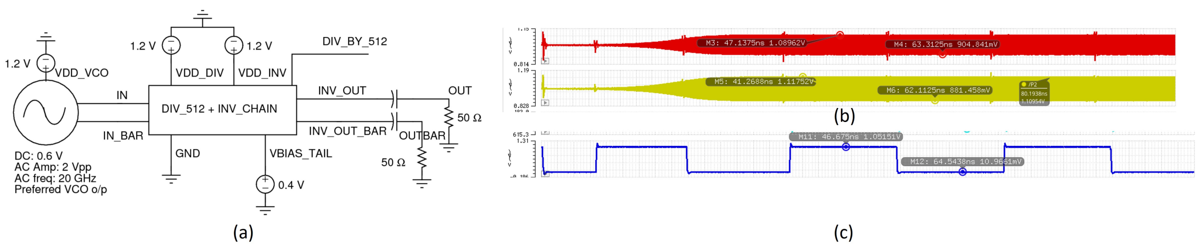

Figure 5.2: (a) Test bench for post layout simulations (b) Differential VCO output at 20 GHz (c) Divided output at 40 MHz

5.2 Object Classification using FMCW Radars

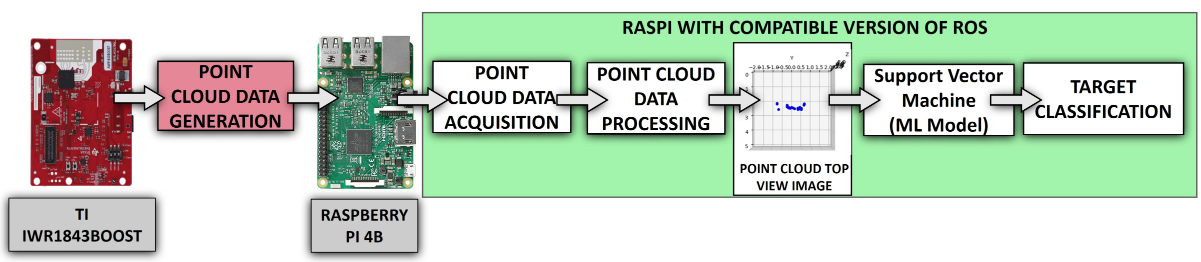

Figure 5.3: Designed system for object classification using FMCW radars

As mentioned earlier, FMCW waves operate at exceptionally high frequencies, allowing them to effectively penetrate atmospheric obstructions like fog, raindrops, and snowflakes. Consequently, there is a compelling case for the development of detection and classification systems based on FMCW radar technology, specifically designed to function reliably in situations of reduced visibility brought about by unfavorable weather conditions. In this study, we developed a system capable of accurately categorizing objects on the road into three main categories: 2-wheelers, 4-wheelers, and pedestrians. The system was designed utilizing TI's IWR1843BOOST FMCW radar, which operates within the frequency range of 77 GHz to 81 GHz, as illustrated in Figure 5.3. The radar was employed to generate point cloud data, which was subsequently wirelessly captured using Python scripts running on a Raspberry Pi 4B. Following data acquisition, a series of processing steps were applied to transform the point cloud data into top-view point cloud images. These images served as input to a support vector machine (SVM) for the precise classification of detected targets into the three specified categories: 2-wheelers, 4-wheelers, and pedestrians.

In the next chapter my research contributions for all the works are discussed. Furthermore, future research that can be developed from the works discussed in this thesis are also discussed.

Chapter 6

Research Contributions & Future Works

This chapter discusses the examines potential avenues for future research and development based on the works presented in this thesis. Furthermore, contributions made by other members of our research group towards this thesis is also acknowledged in this chapter.

6.1 Research Contributions

This thesis presented the core principles underlying the operation of Frequency-Modulated Continuous Wave (FMCW) radars and underscores the significance of Voltage-Controlled Oscillators (VCOs) within the realm of FMCW radar technology. Additionally, the thesis conducts an in-depth examination of emerging techniques that leverage transformer-based resonator tanks to mitigate phase noise in VCOs. These novel methods are elucidated within this document.

Moreover, the transformer-based resonator tank concept is translated into practical application through the development of two distinct VCO designs. The outcomes of these designs are noteworthy, exhibiting substantial enhancements in phase noise performance when compared with existing works in the field. To substantiate the robustness of these designs, extensive post-layout simulations were conducted. These VCO designs were successfully implemented using a 65 nm process technology, signifying their potential impact on the advancement of FMCW radar technology.

6.2 Future Works

The VCOs discussed in this thesis operate at 20 GHz. These VCOs have the versatility to serve as essential components for developing Frequency-Modulated Continuous Wave (FMCW) radars that operate not only at 20 GHz but also at 80 GHz, thereby catering to a range of radar applications across different frequency bands. Moreover, these VCOs can be employed as local oscillators in advanced receiver configurations. Their utilization in such FMCW transceiver topologies contributes to the enhancement of radar systems, facilitating improved signal processing and data acquisition, ultimately leading to enhanced performance and capabilities.

The object classification system created with the use of FMCW radars holds the potential for practical testing in real-world on-road deployments. It can also serve as a valuable benchmarking tool within our research group, aiding in the development and evaluation of other FMCW radar systems. In addition to its current capabilities, there is room for enhancing this system to effectively classify moving objects and predict their velocities. This advancement would not only broaden its utility but also contribute to more comprehensive and accurate object recognition and tracking, thereby bolstering its practicality and applicability in various scenarios.

Related Publications

Accepted Publications

1. S. S. Chatterjee, H. Kambham, A. S. Edakkadan and A. Srivastava, ”Analysis and Design of Low Phase Noise 20 GHz VCO for Frequency Modulated Continuous Wave Chirp Synthesizers in mmWave Radars,” 2023 36th International Conference on VLSI Design and 2023 22nd International Conference on Embedded Systems (VLSID), Hyderabad, India, 2023, pp. 395-400, doi: 10.1109/VLSID57277.2023.00084.

2. S. S. Chatterjee, A. Sahni, H. Kambham, A. Srivastava, ”Design and Analysis of Low Power 20 GHz Colpitts VCO with FoM of 196.26 dBc/Hz,” 2023 IEEE 66th International Midwest Symposium on Circuits and Systems (MWSCAS), Phoenix, Arizona, USA, 2023

Manuscript in progress

S. S. Chatterjee, P. Mahajan, A. S. Edakkadan, J. Benny, Kiruthika K, A. Sahni, Ravi K.S., and A. Srivastava, ”SVM based Object Classification System using FMCW Radar for Road Safety Applications,” IEEE Sensors Journal

Patents Filed

A. Srivastava, Ravi K.S., S. S. Chatterjee, P. Mahajan, A. S. Edakkadan, ”System for classifying and detecting target objects in different weather and lighting conditions using ML”, September 2023, Application No: 202341059920

Bibliography

[1] C. Iovescu and S. Rao. "The Fundamentals of Millimeter Wave Sensors". In: (May 2017).

[2] Junfeng Guan et al. "Through Fog High-Resolution Imaging Using Millimeter Wave Radar". In: *2020 IEEE/CVF Conference on Computer Vision and Pattern Recognition (CVPR)*. 2020, pp. 11461–11470. DOI: 10.1109/CVPR42600.2020.01148.

[3] Sreekiran Samala. "Signal processing and frequency generation in FMCW RADAR". In: *2018 IEEE Custom Integrated Circuits Conference (CICC)*. IEEE. 2018, pp. 1–73.

[4] Christian Waldschmidt, Juergen Hasch, and Wolfgang Menzel. "Automotive radar—From first efforts to future systems". In: *IEEE Journal of Microwaves* 1.1 (2021), pp. 135–148.

[5] Tsuneaki Kenzaka et al. "Importance of vital signs to the early diagnosis and severity of sepsis: association between vital signs and sequential organ failure assessment score in patients with sepsis". In: *Internal Medicine* 51.8 (2012), pp. 871–876.

[6] Shekh M M Islam et al. "Non-Contact Vital Signs Monitoring for Multiple Subjects Using a Millimeter Wave FMCW Automotive Radar". In: *2020 IEEE/MTT-S International Microwave Symposium (IMS)*. 2020, pp. 783–786. DOI: 10.1109/IMS30576.2020.9223838.

[7] Daniel Weyer et al. "A 36.3-to-38.2GHz 216dBc/Hz2 40nm CMOS fractional-N FMCW chirp synthesizer PLL with a continuous-time bandpass delta-sigma time-to-digital converter". In: *2018 IEEE International Solid - State Circuits Conference - (ISSCC)*. 2018, pp. 250–252. DOI: 10.1109/ISSCC.2018.8310278.

[8] Yiyang Shu, Huizhen Jenny Qian, and Xun Luo. "17.4 A 18.6-to-40.1GHz 201.7dBc/Hz FoMT Multi-Core Oscillator Using E-M Mixed-Coupling Resonance Boosting". In: *2020 IEEE International Solid- State Circuits Conference - (ISSCC)*. 2020, pp. 272–274. DOI: 10.1109/ISSCC19947.2020.9063100.

[9] Abhishek Bhat and Nagendra Krishnapura. "26.3 A 25-to-38GHz, 195dB FoMT LC QVCO in 65nm LP CMOS Using a 4-Port Dual-Mode Resonator for 5G Radios". In: *2019 IEEE International Solid- State Circuits Conference - (ISSCC)*. 2019, pp. 412–414. DOI: 10.1109/ISSCC.2019.8662502.

[10] D.B. Leeson. "A simple model of feedback oscillator noise spectrum". In: *Proceedings of the IEEE* 54.2 (1966), pp. 329–330. DOI: 10.1109/PROC.1966.4682.

[11] J.J. Rael and A.A. Abidi. "Physical processes of phase noise in differential LC oscillators". In: *Proceedings of the IEEE 2000 Custom Integrated Circuits Conference (Cat. No.00CH37044)*. 2000, pp. 569–572. DOI: 10.1109/CICC.2000.852732.

[12] E. Hegazi, H. Sjoland, and A.A. Abidi. "A filtering technique to lower LC oscillator phase noise". In: *IEEE Journal of Solid-State Circuits* 36.12 (2001), pp. 1921–1930. DOI: 10.1109/4.972142.

[13] Masoud Babaie and Robert Bogdan Staszewski. "A Class-F CMOS Oscillator". In: *IEEE Journal of Solid-State Circuits* 48.12 (2013), pp. 3120–3133. DOI: 10.1109/JSSC.2013.2273823.

[14] David Murphy, Hooman Darabi, and Hao Wu. "Implicit Common-Mode Resonance in LC Oscillators". In: *IEEE Journal of Solid-State Circuits* 52.3 (2017), pp. 812–821. DOI: 10.1109/JSSC.2016.2642207.

[15] Masoud Babaie and Robert Bogdan Staszewski. "An Ultra-Low Phase Noise Class-F 2 CMOS Oscillator With 191 dBc/Hz FoM and Long-Term Reliability". In: *IEEE Journal of Solid-State Circuits* 50.3 (2015), pp. 679–692. DOI: 10.1109/JSSC.2014.2379265.

[16] A. Hajimiri and T.H. Lee. "A general theory of phase noise in electrical oscillators". In: *IEEE Journal of Solid-State Circuits* 33.2 (1998), pp. 179–194. DOI: 10.1109/4.658619.

[17] Chee Cheow Lim et al. "An Inverse-Class-F CMOS Oscillator With Intrinsic-High-Q First Harmonic and Second Harmonic Resonances". In: *IEEE Journal of Solid-State Circuits* 53.12 (2018), pp. 3528–3539. DOI: 10.1109/JSSC.2018.2875099.

[18] Seok-Ju Yun et al. "A 1mW current-reuse CMOS differential LC-VCO with low phase noise". In: *ISSCC. 2005 IEEE International Digest of Technical Papers. Solid-State Circuits Conference, 2005*. 2005, 540–616 Vol. 1. DOI: 10.1109/ISSCC.2005.1494108.

[19] Masoud Babaie, Mina Shahmohammadi, and Robert Bogdan Staszewski. *RF CMOS Oscillators for Modern Wireless Applications*. CRC Press, 2022.

[20] Hao Guo et al. "26.2 A 0.08mm2 25.5-to-29.9GHz Multi-Resonant-RLCM-Tank VCO Using a Single-Turn Multi-Tap Inductor and CM-Only Capacitors Achieving 191.6dBc/Hz FoM and 130kHz 1/f3 PN Corner". In: *2019 IEEE International Solid- State Circuits Conference - (ISSCC)*. 2019, pp. 410–412. DOI: 10.1109/ISSCC.2019.8662470.

[21] Hao Guo et al. "A Millimeter-Wave CMOS VCO Featuring a Mode-Ambiguity-Aware Multi-Resonant-RLCM Tank". In: *IEEE Transactions on Circuits and Systems I: Regular Papers* 69.1 (2022), pp. 172–185. DOI: 10.1109/TCSI.2021.3096196.

[22] Omid Esmaeeli et al. "A Transformer-Based Technique to Improve Tuning Range and Phase Noise of a 20–28GHz LCVCO and a 51–62GHz Self-Mixing LCVCO". In: *IEEE Transactions on Circuits and Systems I: Regular Papers* 69.6 (2022), pp. 2351–2363. DOI: 10.1109/TCSI.2022.3158656.

[23] Nusrat Jahan, Adel Barakat, and Ramesh K. Pokharel. "Design of Low Phase Noise VCO Considering C/L Ratio of LC Resonator in 0.18-m CMOS Technology". In: *IEEE Transactions on Circuits and Systems II: Express Briefs* 68.12 (2021), pp. 3513–3517. DOI: 10.1109/TCSII.2021.3079309.

[24] Zhiwei Zong, Giovanni Mangraviti, and Piet Wambacq. "Low 1/f3 Noise Corner LC-VCO Design Using Flicker Noise Filtering Technique in 22nm FD-SOI". In: *IEEE Transactions on Circuits and Systems I: Regular Papers* 67.5 (2020), pp. 1469–1480. DOI: 10.1109/TCSI.2020.2970267.

[25] Shita Guo et al. "A Low-Voltage Low-Phase-Noise 25-GHz Two-Tank Transformer-Feedback VCO". In: *IEEE Transactions on Circuits and Systems I: Regular Papers* 65.10 (2018), pp. 3162–3173. DOI: 10.1109/TCSI.2018.2815843.

[26] Harikrishna Kambham et al. "Analysis and Design of Low Phase Noise 20 GHz VCO for Frequency Modulated Continuous Wave Chirp Synthesizers in mmWave Radars". In: *2023 36th International Conference on VLSI Design and 2023 22nd International Conference on Embedded Systems (VLSID)*. 2023, pp. 395–400. DOI: 10.1109/VLSID57277.2023.00084.

[27] R. Aparicio and A. Hajimiri. “A noise-shifting differential Colpitts VCO”. In: *IEEE Journal of Solid-State Circuits* 37.12 (2002), pp. 1728–1736. DOI: 10.1109/JSSC.2002.804354.

[28] R. Aparicio and A. Hajimiri. “A CMOS differential noise-shifting Colpitts VCO”. In: *2002 IEEE International Solid-State Circuits Conference. Digest of Technical Papers (Cat. No.02CH37315)*. Vol. 1. 2002, 288–289 vol.1. DOI: 10.1109/ISSCC.2002.993045.

[29] Xiaoyong Li, S. Shekhar, and D.J. Allstot. “G/sub m/-boosted common-gate LNA and differential colpitts VCO/QVCO in 0.18-/spl mu/m CMOS”. In: *IEEE Journal of Solid-State Circuits* 40.12 (2005), pp. 2609–2619. DOI: 10.1109/JSSC.2005.857426.

[30] Salvatore Galeone and Michael Peter Kennedy. “A comparison of simulation strategies for estimating phase noise in oscillators”. In: *2017 13th Conference on Ph.D. Research in Microelectronics and Electronics (PRIME)*. 2017, pp. 213–216. DOI: 10.1109/PRIME.2017.7974145.

[31] Alessandro Franceschin et al. “A 19.5-GHz 28-nm Class-C CMOS VCO, With a Reasonably Rigorous Result on 1/f Noise Upconversion Caused by Short-Channel Effects”. In: *IEEE Journal of Solid-State Circuits* 55.7 (2020), pp. 1842–1853. DOI: 10.1109/JSSC.2020.2987702.

[32] Wen-Cheng Lai and Sheng-Lyang Jang. “A CMOS Colpitts Voltage-Controlled Oscillator with Bias-Free pMOSFET Tails”. In: *2020 IEEE Asia-Pacific Microwave Conference (APMC)*. 2020, pp. 666–668. DOI: 10.1109/APMC47863.2020.9331625.

[33] Dinesh Kumar B., Hitesh Shrimali, and Nagarjuna Nallam. “A Low-Power Quadrature LC-Oscillator Using Core-and-Coupling Current-Reuse”. In: *2021 IEEE International Symposium on Circuits and Systems (ISCAS)*. 2021, pp. 1–5. DOI: 10.1109/ISCAS51556.2021.9401110.

[34] Yuri Lu et al. “A 23.4-27.6 GHz “Zig-Zag” VCO with Continuous Frequency Switching for FMCW Radars”. In: *2022 IEEE International Symposium on Circuits and Systems (ISCAS)*. 2022, pp. 3355–3358. DOI: 10.1109/ISCAS48785.2022.9937550.

[35] Daniel Reiter et al. “A Low Phase Noise, Wide Tuning Range 20GHz Magnetic-Coupled Hartley-VCO in a 28nm CMOS Technology”. In: *2019 IEEE Radio and Wireless Symposium (RWS)*. 2019, pp. 1–3. DOI: 10.1109/RWS.2019.8714258.